NOAA Technical Memorandum ERL WPL-105

IMPROVED ESTIMATES OF HF RADIOWAVE FIELD STRENGTH NEAR A LAND-SEA INTERFACE

R. M. Jones

Wave Propagation Laboratory
Boulder, Colorado
November 1982

noaa NATIONAL OCEANIC AND ATMOSPHERIC ADMINISTRATION / Environmental Research Laboratories

NOAA Technical Memorandum ERL WPL-105

IMPROVED ESTIMATES OF HF RADIOWAVE FIELD STRENGTH NEAR A LAND-SEA INTERFACE

R. M. Jones

Wave Propagation Laboratory
Boulder, Colorado
November 1982

UNITED STATES
DEPARTMENT OF COMMERCE
Malcolm Baldrige,
Secretary

NATIONAL OCEANIC AND
ATMOSPHERIC ADMINISTRATION
John V. Byrne,
Administrator

Environmental Research
Laboratories
George H. Ludwig
Director

CONTENTS

IMPROVED ESTIMATES OF HF RADIOWAVE FIELD STRENGTH NEAR A LAND-SEA INTERFACE

R. M. Jones

ABSTRACT

Results of other researchers are extended to give the detailed behavior of mixed-path (land-sea or sea-land) propagation near the land-sea interface. It is shown that the mechanism for groundwave-mode coupling at the land-sea interface is edge-diffraction, and that near the shoreline the direct edge-diffracted wave can make a significant contribution to the field. It is further argued that, for sea-to-land propagation for an elevated observer, the sea-type groundwave modes extend over land, and there is a shadow zone for the land-type groundwave modes excited at the shoreline. Corresponding results hold for land-to-sea propagation.

1. INTRODUCTION

When we measure ocean wave parameters with our Coastal Ocean Dynamics Applications Radar (CODAR) (Barrick et al., 1977) the propagation of the radio waves from the land-based radar to the ocean target and back depends on how radio waves propagate across a land-sea boundary. Of particular interest is how the echo strength depends on the location of the transmitting and receiving antennas relative to the land-sea boundary.

Figure 1 shows the geometry of the problem. For large enough distances, the propagation is by groundwave propagation rather than line-of-sight rays. Because the propagation is reciprocal, I consider here only one-way propagation from the scattering patch on the sea surface to the radar on the land. For the round-trip path, the amplitude (in decibels) and the phase are simply doubled. To increase the generality, however, I consider that both the source (over the sea) and the observer (over the land) are elevated. I consider special cases later.

The mixed-path problem in radio wave propagation over the earth has received a great deal of attention. Using the compensation theorem, Wait (1961) has calculated coupling coefficients among the groundwave modes at the land-sea boundary. Wait and Walters (1963) and Hill and Wait (1981) have calculated some numerical examples. Figure 2 shows an example of such calculations for conditions relevant to our CODAR measurements.

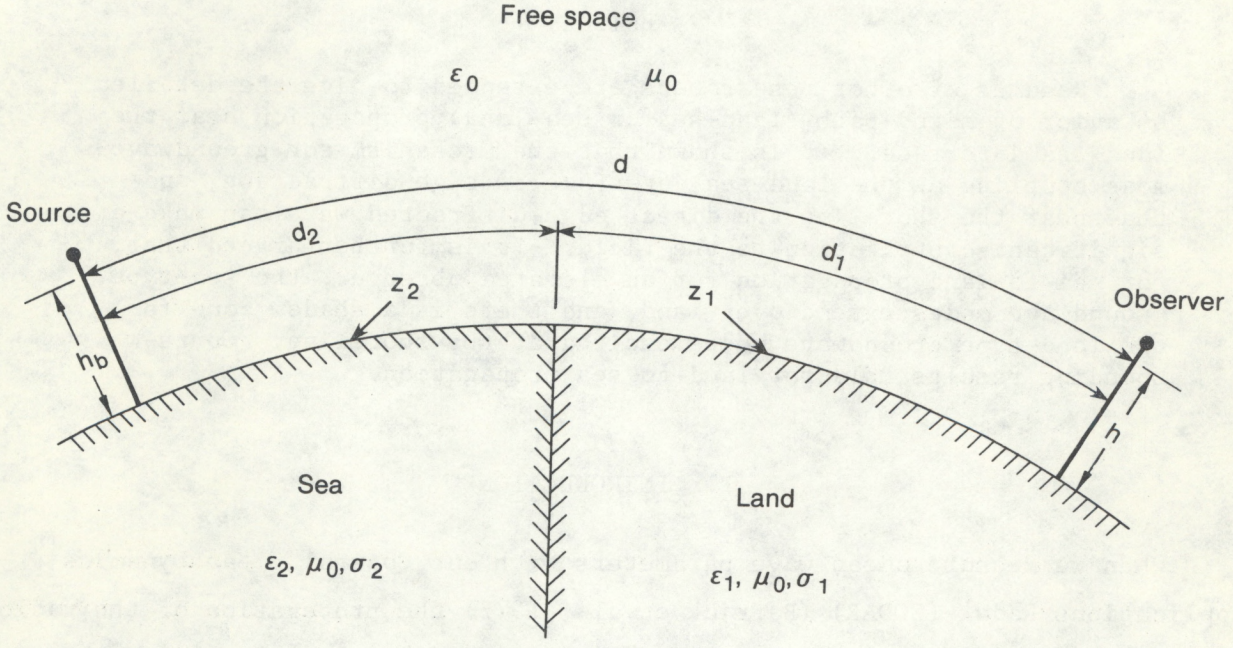

Figure 1. Geometry for propagation over a mixed land-sea path. The source is above the sea (characterized by a permittivity ε_2 and conductivity σ_2, or a surface impedance z_2), and the observer is above land (characterized by a permittivity ε_1 and conductivity σ_1, or a surface impedance z_1). The conductivity of free space is zero, and μ_o is the magnetic permeability through the medium.

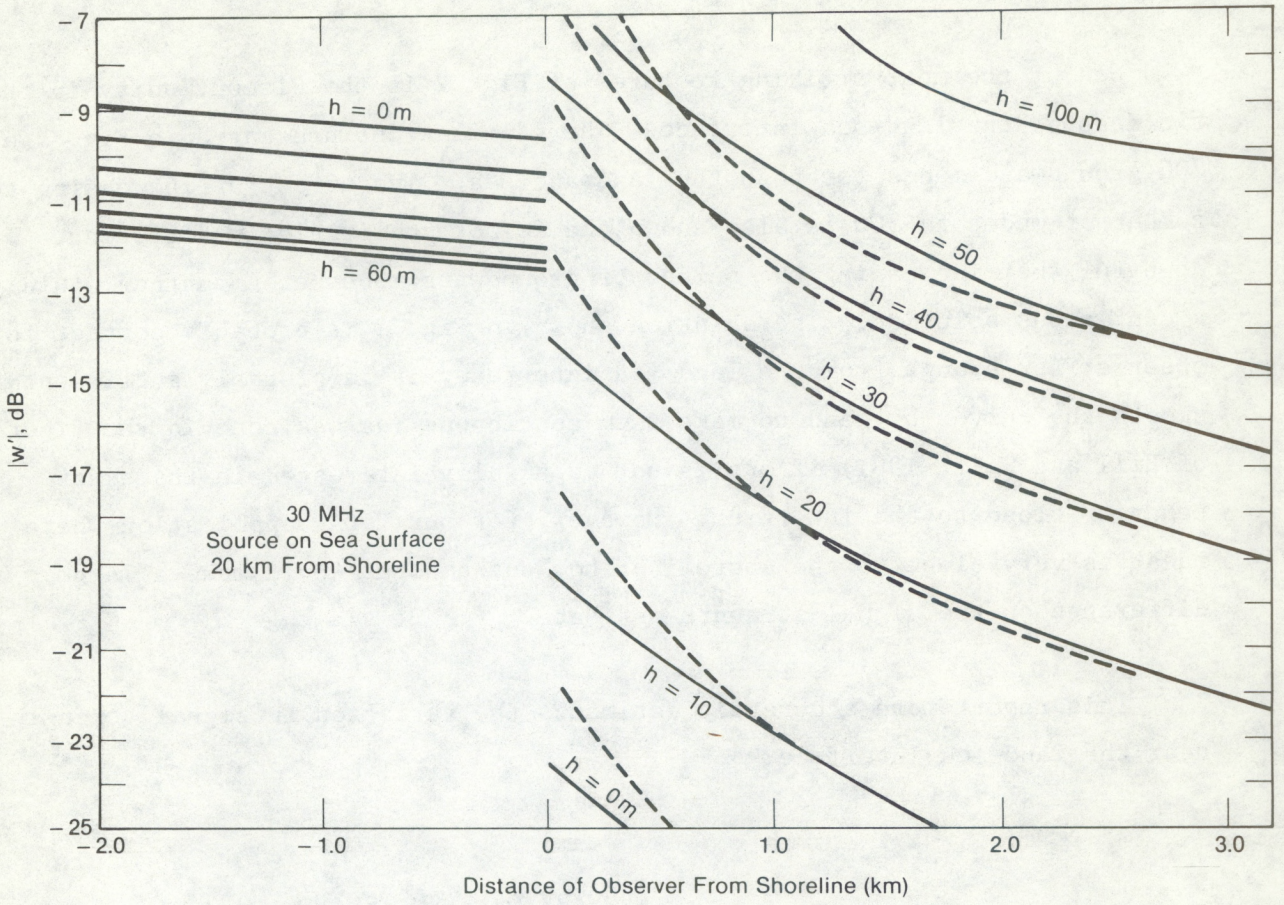

Figure 2. Mixed-path groundwave propagation using the groundwave-mode conversion formulas of Hill and Wait (1981). The field has been normalized to the free-space field above a flat, perfect conductor. The source is a vertical electric dipole on the surface of the sea 20 km from the shoreline. The frequency is 30 MHz. The calculations were made with the program MPHGAIN from David Hill (National Bureau of Standards; Boulder, CO). The discontinuity in the field above the shoreline is not considered realistic. The solid lines are for 200 groundwave modes, the dashed lines for 500 modes.

One of the most striking features of Fig. 2 is the discontinuity in the field above the land-sea interface. The calculations presented in Fig. 2 use 200 groundwave modes for both the land and sea. The effect of increasing the number of modes to 500 is also shown and is not qualitatively different. It is doubtful that increasing the number of groundwave modes even further would yield a continuous solution. The solution shown in Fig. 2 is probably correct for an observer far enough from the land-sea interface; it is probably sufficient to smooth the curves by hand to make them continuous (as was done in the figures of Hill and Wait, 1981) if one is not especially interested in the exact behavior close to the interface. However, for our CODAR application where our radar is very close to the shoreline, how one smooths would make a large difference on the signal-strength estimate.

This report more accurately estimates the variation in signal strength near the land-sea interface.

2. SUMMARY OF RESULTS

1) Edge-diffraction is the mechanism for coupling of groundwave modes at a land-sea boundary. Combining the complex-height, creeping-ray representation of groundwave modes with an edge-diffraction coefficient of Kaminetzky and Keller (1972) gives the mixed-path groundwave propagation formulas of Hill and Wait (1981).

2) For propagation from sea to land, the sea-type groundwave modes do not stop at the shoreline, but continue over land for some distance for an elevated observer. The higher the observer, the farther the modes extend over the land. The lower order modes continue farther than higher order modes before they are cut off. For calculations here, the modes are cut off abruptly, but an analysis of the shadow boundary transition would show a more gradual fading of each mode. For propagation from land to sea, the corresponding results hold.

3) For propagation from sea to land, the land-type groundwave modes excited at the shoreline are not detectable by an elevated observer who is too close to the shoreline. This shadow zone extends farther over land from the shoreline the higher the observer and the lower the order of the groundwave mode. For purposes of calculations here, the shadow zone is considered to have a sharp boundary for each groundwave mode, but an analysis of the shadow boundary transition would show a more gradual change. For propagation from land to sea, the corresponding results hold.

4) Close to the shoreline, there is a direct edge-diffracted wave that contributes to the total field. For sea-to-land propagation, the edge-diffracted wave is an alternate representation of the field to the land-type groundwave, and is more accurate near the shoreline. For land-to-sea propagation, the corresponding results hold. Which of these waves dominates the received field strength depends on the height of the observer and his distance from the shoreline, as shown on the accompanying plots.

The results presented here apply not only to a land-sea boundary, but to any abrupt change in the surface impedance of the ground.

3. THE CREEPING-RAY REPRESENTATION OF GROUNDWAVE MODES

Keller (1962) showed how surface-diffracted waves could be represented by creeping rays (rays that follow geodesics on the surface). Levy and Keller (1959) derived the diffraction coefficients necessary to calculate field strengths for surface-diffracted waves. Jones (1968) recognized that groundwave modes on the Earth correspond to surface-diffracted waves and showed the equivalence of the surface-diffracted waves with the groundwave-mode sums of Watson (1918), Bremmer (1949), and Wait (1960). He also showed that representing the creeping rays as rays that have a particular complex height (that depends on the groundwave-mode propagation constant) gives a closer representation of the groundwave modes than having the creeping rays on the ground. Table 1 summarizes the results of Jones (1968) and defines all of the terms it uses. His groundwave excitation coefficient and shedding coefficient together replace, but are equivalent to, the diffraction coefficient of Levy and Keller (1959).

Table 1. Propagation, excitation, and radiation properties of the groundwave

Propagation along the ground Each groundwave mode has a characteristic angular propagation constant ν. ($e^{-i\nu\alpha}$ gives the change in field strength of the groundwave mode in a central earth angle α, and ν is complex to give both amplitude and phase.) It can be represented by a surface diffracted ray at a complex height ν/k-a above the ground.	Angular propagation constant $\nu = ka + \left(\frac{ka}{2}\right)^{1/3} t$ where k is the propagation constant of free space. a is the radius of the earth. t is a root of $w_1'(t) = q\, w_1(t)$ $w_1(t) = \sqrt{\pi}\,(Bi(t) - i\,Ai(t))$ Ai and Bi are Airy functions $q = -i\left(\frac{ka}{2}\right)^{1/3} \frac{Z_g}{\eta_o} = -i\left(\frac{ka}{2}\right)^{1/3} \sqrt{\left(\frac{k_2}{k}\right)^2 - \left(\frac{\nu}{ka}\right)^2} \Big/ \left(\frac{k_2}{k}\right)^2 \approx -i\left(\frac{ka}{2}\right)^{1/3} \sqrt{\left(\frac{k_2}{k}\right)^2 - 1} \Big/ \left(\frac{k_2}{k}\right)^2$ Z_g is the surface impedance of the ground. η_o is the impedance of free space. k_2 is the (complex) propagation constant of the ground.
Excitation of the groundwave The groundwave is excited by a ray tangent to the surface diffracted ray. The excitation coefficient equals the ratio of the transverse electric field of the groundwave at the point of excitation to that of the radiation field of the source at the same point. ℓ is the distance from the source to the excitation point. h is the height of the source above the ground.	Excitation coefficient $D_\nu(\ell) = -\frac{2i\sqrt{\pi}}{t - q^2}\, w_1(0)/w_1(t)^2\, e^{i\pi/4}\, (-y)^{1/4}\, e^{i2/3(-y)^{3/2}}\, w_1(y)$ where $\frac{2}{3}(-y)^{3/2} = k\ell - \nu\tan^{-1}\frac{k}{\nu}\ell$ special cases: $D_\nu = \lim_{\ell\to\infty} D_\nu(\ell) = -\frac{2i\sqrt{\pi}}{t - q^2}\, w_1(0)/w_1(t)^2$ for small ℓ, $D_\nu(\ell) \approx -\frac{2i\sqrt{\pi}}{t - q^2}\, w_1(0)/w_1(t)^2\, e^{i\pi/4} \left(\frac{ka}{2}\right)^{1/6} \left(\frac{\ell}{a}\right)^{1/2} e^{ik\ell} e^{-i\nu\tan^{-1}\frac{k}{\nu}\ell}\, w_1\left(t - \left(\frac{2}{ka}\right)^{1/3} kh\right)$ where $h = \sqrt{\left(\frac{\nu}{k}\right)^2 + \ell^2} - a \approx \frac{\nu}{k} - a + \frac{1}{2}\frac{k}{\nu}\ell^2$ $\lim_{\ell\to 0} D_\nu(\ell) = -\frac{2i\sqrt{\pi}}{t - q^2}\, w_1(0)/w_1(t)^2 \left(\frac{ka}{2}\right)^{1/6} \left(\frac{\ell}{a}\right)^{1/2} e^{i\pi/4}\, w_1(0)$
Radiation from the groundwave The groundwave sheds rays (radiates) tangentially from the surface diffracted ray. The shedding coefficient equals the ratio of the transverse electric field a distance ℓ from the point of shedding to that of the groundwave at the point of shedding exclusive of the phase integral and azimuthal focusing contributions (that is, it includes only elevation focusing). h is the height of the observation point above the ground.	Shedding coefficient $S(\ell) = \left(\frac{2}{ka}\right)^{1/6} \left(\frac{a}{\ell}\right)^{1/2} (-y)^{1/4}\, e^{i2/3(-y)^{3/2}}\, w_1(y)/w_1(0)$ where $\frac{2}{3}(-y)^{3/2} = k\ell - \nu\tan^{-1}\frac{k}{\nu}\ell$ special cases: $\lim_{\ell\to\infty} S(\ell) = \left(\frac{2}{ka}\right)^{1/6} e^{-i\pi/4} \left(\frac{a}{\ell}\right)^{1/2} / w_1(0)$ $\lim_{\ell\to 0} S(\ell) = e^{ik\ell} e^{-i\nu\tan^{-1}\frac{k}{\nu}\ell}\, w_1\left(t - \left(\frac{2}{ka}\right)^{1/3} kh\right) / w_1(0)$ where $h = \sqrt{\left(\frac{\nu}{k}\right)^2 + \ell^2} - a \approx \frac{\nu}{k} - a + \frac{1}{2}\frac{k}{\nu}\ell^2$ $S(0) = 1$

After Jones, 1968; corrected 8 May 1972.

Physically, a groundwave mode is a ground-reflected wave for which the angle of incidence is such that the reflection coefficient is infinite. An infinite reflection coefficient allows the boundary conditions to be satisfied by a reflected wave in the absence of an incident wave; therefore, a groundwave mode can propagate away from where it was produced. It is a reflected wave that satisfies the boundary conditions without an incident wave.

Mathematically, groundwave modes arise from a residue expansion of a contour integral of a ground-reflected wave. The angle of incidence is related to the independent variable of integration in that contour integral; the poles of the integrand for the residue expansion are the poles of the ground reflection coefficient. The infinite ground reflection coefficient connects the mathematical with the physical interpretation of a groundwave mode.

Figure 3 shows the geometry for calculating excitation of and radiation (shedding) from a groundwave mode. Jones (1968) shows that the vertical electric field at the receiver is

$$E = \left[i \frac{Ids\omega\mu_o}{4\pi} \frac{e^{-ik\ell_T}}{\ell_T} \cos\beta_T \right] \left[D_\nu(\ell_T) \right] \left[e^{-i\nu(\theta-\beta_T-\beta_R)} \right]$$

$$\left[S(\ell) \right] \left[e^{-ik\ell} \right] \left[\sqrt{\frac{\nu}{k} \frac{\sin\beta_T}{r \sin\theta}} \right] \left[\cos\beta_R \right], \qquad (3.1)$$

where the 7 factors are, respectively, (1) the incident field from the transmitter at the point of excitation of the groundwave, (2) the groundwave excitation coefficient $D_\nu(\ell_T)$, (3) the phase integral of the surface-diffracted ray from the point of excitation to the point of shedding, (4) the shedding coefficient $S(\ell)$, (5) the phase integral from the point of shedding to the receiver, (6) a convergence factor due to azimuthal focusing, and (7) the pattern factor of the receiving antenna (a vertical dipole). The excitation and shedding coefficients are given in Table 1. Figure 3 can be used to evaluate all of the geometrical quantities in (3.1) in terms of known quantities. The quantity Ids is the current moment of the vertical dipole transmitting antenna.

In the following sections I will make similar calculations to calculate mode coupling at the land-sea boundary.

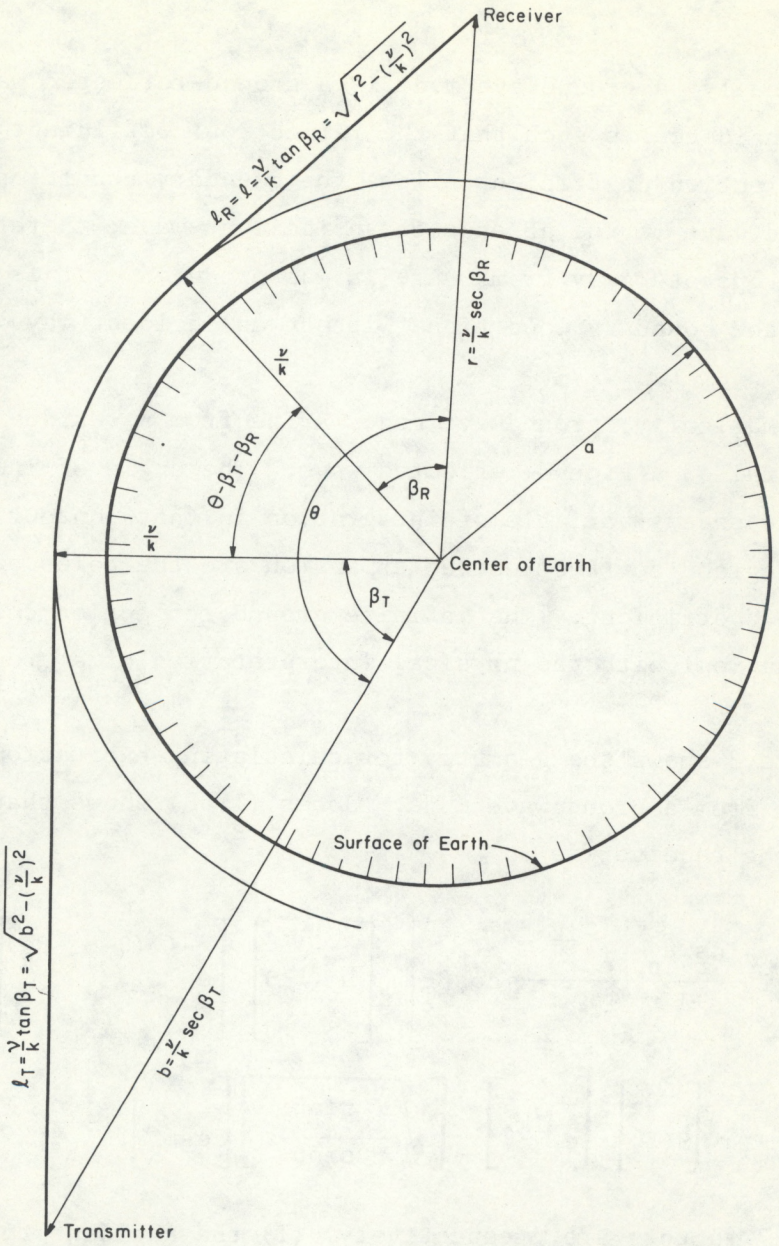

Figure 3. Representation of a groundwave mode by a surface-diffracted ray at a complex height $\nu/k-a$. The sphere of complex radius ν/k is a caustic for the groundwave mode. From Jones (1968; Fig. 3).

4. COUPLING OF GROUNDWAVE MODES BY EDGE DIFFRACTION

As was mentioned in the introduction, over the sea we have one set of groundwave modes and over the land another set. A groundwave mode incident from the sea on the sea-land interface will excite groundwave modes appropriate to propagation over the land. One possible mechanism for conversion of a sea-type groundwave mode to a land-type groundwave mode is edge-diffraction. As we shall see, the hypothesis that edge-diffraction is the correct mechanism leads to agreement with independent calculations.

Briefly, the edge-diffraction mechanism for coupling groundwave modes works as follows. The field of the sea-type groundwave mode incident on the land-sea interface is calculated in the usual way as though there were a receiver there, but ignoring the pattern factor of the receiving antenna. The field strength is then assumed to be that of an incident wave on the land-sea interface at the appropriate angle of incidence. Using the appropriate scattering coefficient, we then calculate the scattered field from the land-sea interface. (This will be a cylindrical wave with a pattern factor determined by the scattering coefficient.) We then treat that cylindrical wave as a virtual source that excites a land-type groundwave mode in the usual way.

Figure 4 shows a drawing of the ray structure for this process. However, Fig. 4 is inaccurate in that all four straight-line ray segments should be tangent to the circular surface-diffracted rays. This is impossible to draw for the two rays that connect at the land-sea interface, even though the configuration is possible with complex rays. Figure 5 shows another representation of this process. Although it represents the surface-diffracted waves by creeping rays below the Earth's surface, and seems to require rays to penetrate the surface of the Earth, it correctly shows the four straight-line rays tangent to the creeping rays, and it can be used to calculate coupling of groundwave modes at the land-sea interface.

We again consider a vertical electric dipole source. Then following the example in Section 3, the vertical electric field as seen by the observer in Fig. 5 is

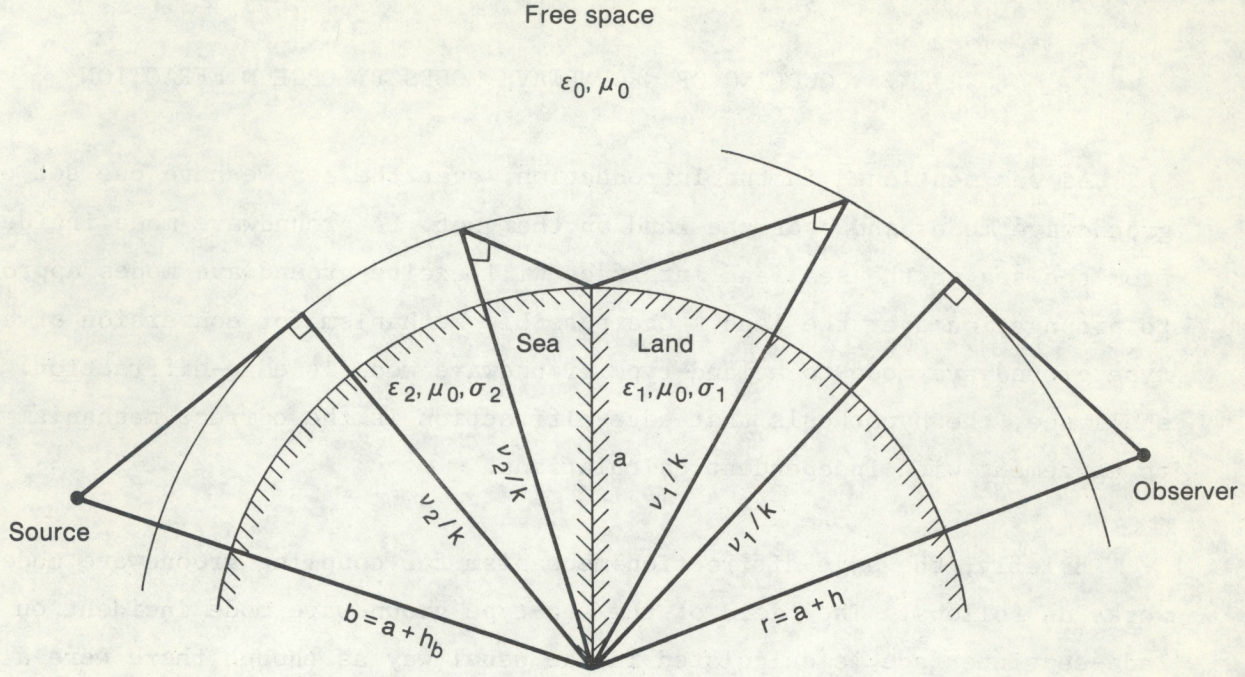

Figure 4. Geometry to represent coupling of groundwave modes at a land-sea boundary by edge-diffraction. The impossibility of drawing a ray from the land-sea interface that is tangent to the caustic for the groundwave mode disqualifies this figure as being useful for making calculations.

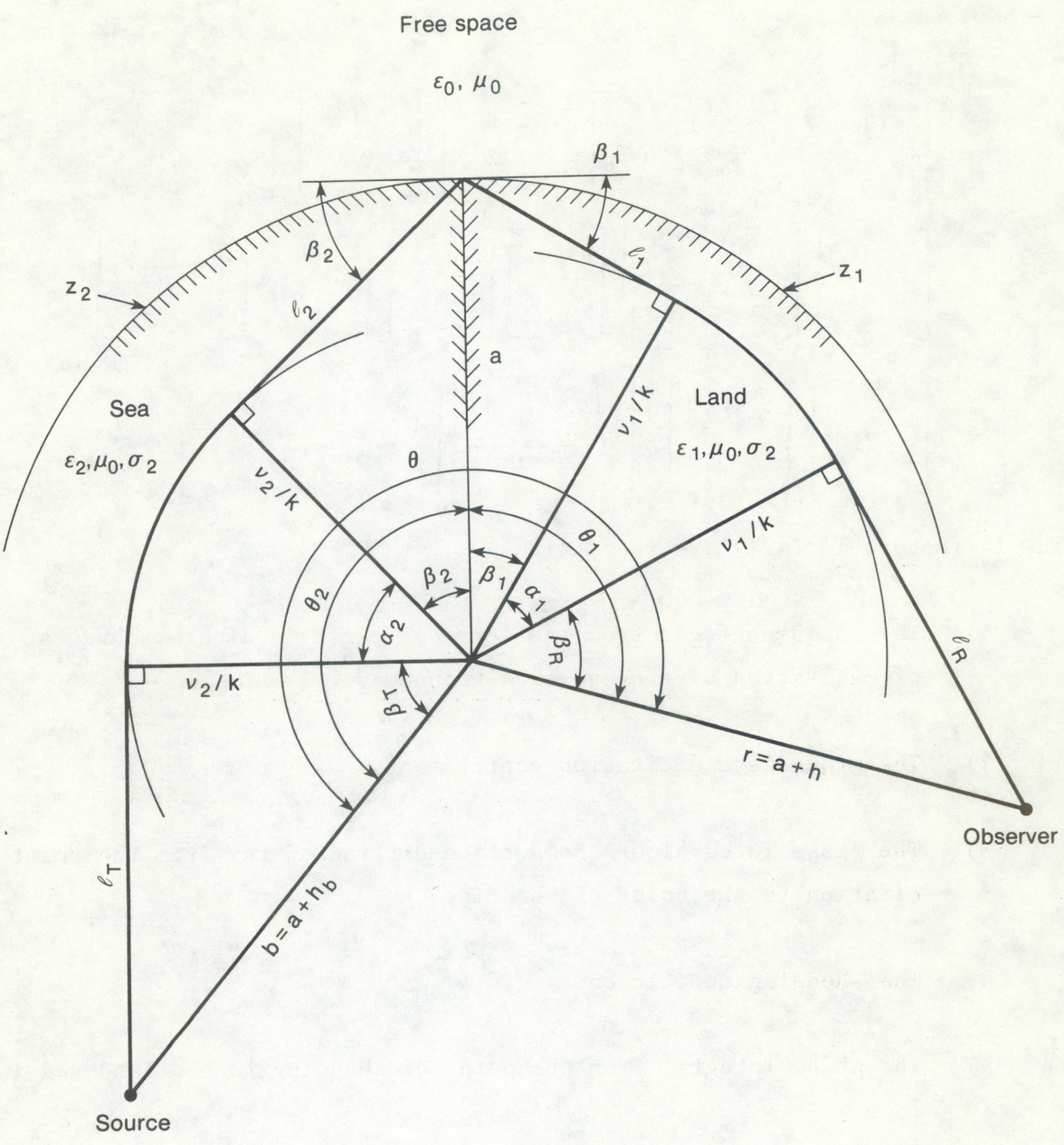

Figure 5. Geometry to represent coupling of groundwave modes at a land-sea boundary by edge-diffraction. Although the rays are unrealistically represented as being below the Earth's surface, the correct geometrical relationships allow this figure to be useful for making calculations.

$$E = \left[i \frac{Ids\omega\mu_o}{4\pi} \frac{e^{-ik\ell_T}}{\ell_T} \cos\beta_T \right] \left[D_{\nu_2}(\ell_T) \right] \left[e^{-i\nu_2\alpha_2} \right] \left[S_{\nu_2}(\ell_2) \right]$$

$$\left[e^{-ik\ell_2} \right] \left[D_E(-\beta_1, -\beta_2) \right] \left[\frac{1}{\sqrt{k\ell_1}} \right] \left[e^{-ik\ell_1} \right] \left[D_{\nu_1}(\ell_1) \right] \left[e^{-i\nu_1\alpha_1} \right]$$

$$\left[S_{\nu_1}(\ell_R) \right] \left[e^{-ik\ell_R} \right] \left[\sqrt{\frac{\nu_2}{k} \frac{\sin\beta_T}{r \sin\theta}} \right] \left[\cos\beta_R \right] . \qquad (4.1)$$

The 14 factors in (4.1) are respectively

1) The incident field from the vertical electric dipole source at the point of excitation of the sea-type groundwave.

2) The groundwave excitation coefficient.

3) The phase integral of the surface-diffracted ray from the point of excitation to the point of shedding.

4) The shedding coefficient.

5) The phase integral from the point of shedding to the land-sea interface.

6) The edge-diffraction coefficient for an incident grazing angle $-\beta_2$ and a scattering angle $-\beta_1$.

7) The geometrical spreading factor for the cylindrical wave scattering from the land-sea interface.

8) The phase integral from the land-sea interface to the point of excitation of the land-type groundwave mode.

9) The groundwave excitation coefficient.

10) The phase integral of the surface-diffracted ray from the point of excitation to the point of shedding.

11) The shedding coefficient.

12) The phase integral from the point of shedding to the observer.

13) A convergence factor to account for azimuthal focusing.

14) The pattern factor of the receiving antenna (a vertical dipole).

Table 1 gives the formulas for the excitation and shedding coefficients; I is the peak current in the source antenna; ds is the length of the source antenna; and the formula for the edge diffraction coefficient D_E is given in Section 5. All of the other quantities in (4.1) can be found from the geometry in Fig. 5 in terms of known quantities. These are given in Appendix A.

We can use Table 1 and (A.1) through (A.10) from Appendix A in (4.1). After some algebra, this gives

$$E = \left[\sqrt{2}\left(\frac{ka}{2}\right)^{1/3}\left(\frac{y_b - t_2}{k^2b^2 - \nu_2^2}\right)^{1/4}\right]\left[\sqrt{2}\left(\frac{ka}{2}\right)^{1/3}\left(\frac{-t_1}{k^2a^2 - \nu_1^2}\right)^{1/4}\right]\left[\sqrt{2}\left(\frac{ka}{2}\right)^{1/3}\left(\frac{y - t_1}{k^2r^2 - \nu_1^2}\right)^{1/4}\right]$$

$$\frac{\nu_1}{kr}\left(\frac{a}{r}\right)^{1/2}\left(\frac{\nu_2}{kb}\right)^{3/2} 2i\,\frac{Ids\omega\mu_o}{4\pi a\theta}\sqrt{\frac{\pi\left(\frac{ka}{2}\right)^{1/3}\theta^2}{i\sin\theta}}\,\frac{e^{i\pi/4}}{i}\left(\frac{2}{ka}\right)^{1/3}(2\pi)^{1/2} D_E$$

$$\frac{e^{-i\nu_2\theta_2}}{t_2 - q_2^2}\,\frac{e^{-i\nu_1\theta_1}}{t_1 - q_1^2}\,\frac{w_1(t_2 - y_b)}{w_1(t_2)}\,\frac{w_1(t_1 - y)}{w_1(t_1)}, \qquad (4.2)$$

where Appendix B gives the formulas for y_b, y, ν_2, ν_1, q_2, q_1, t_2, and t_1.

We can make some approximations because the first term in (B.3) and in (B.4) is much larger than the second term. [At HF (10 to 30 MHz) ka is about 10^6, and t_2 and t_1 vary from order unity to about 50 for the first two hundred groundwave

modes. For high enough mode number, the approximation would eventually not be valid, but when that happens, (4.2) will no longer be valid because its validity depends on the first term in (B.3) and (B.4) being much larger than the second term.] With this approximation, the second factor in square brackets in (4.2) is approximately unity, and we can use

$$\nu_1 \tilde{\sim} \nu_2 \tilde{\sim} ka \tag{4.3}$$

nearly everywhere but in exponential terms. Thus, (4.2) is approximately

$$E = \left[\sqrt{2}\left(\frac{ka}{2}\right)^{1/3}\left(\frac{y_b - t_2}{k^2 b^2 - \nu_2^2}\right)^{1/4}\right]\left[\sqrt{2}\left(\frac{ka}{2}\right)^{1/3}\left(\frac{y - t_1}{k^2 r^2 - \nu_1^2}\right)^{1/4}\right]\left(\frac{a}{r}\right)^{3/2}\left(\frac{a}{b}\right)^{3/2}$$

$$2i\,\frac{Ids\omega\mu_o}{4\pi a\theta}\sqrt{\frac{\pi\left(\frac{ka}{2}\right)^{1/3}\theta^2}{i\sin\theta}}\,\frac{e^{i\pi/4}}{i}\left(\frac{2}{ka}\right)^{1/3}(2\pi)^{1/2}D_E$$

$$\frac{e^{-i\nu_2\theta_2}}{t_2 - q_2^2}\,\frac{e^{-i\nu_1\theta_1}}{t_1 - q_1^2}\,\frac{w_1(t_2 - y_b)}{w_1(t_2)}\,\frac{w_1(t_1 - y)}{w_1(t_1)}\,. \tag{4.4}$$

It is usual to normalize E to the free-space field above a flat, perfect conductor. We can take this to be

$$E_o = 2i\,\frac{Ids\omega\mu_o}{4\pi}\,\frac{e^{-ika\theta}}{a\theta}\,. \tag{4.5}$$

Dividing (4.4) by (4.5) and using (B.3), (B.4), and (A.11) gives

$$E/E_o = \left[\sqrt{2}\left(\frac{ka}{2}\right)^{1/3}\left(\frac{y_b - t_2}{k^2 b^2 - \nu_2^2}\right)^{1/4}\right]\left[\sqrt{2}\left(\frac{ka}{2}\right)^{1/3}\left(\frac{y - t_1}{k^2 r^2 - \nu_1^2}\right)^{1/4}\right]\left(\frac{a}{r}\right)^{3/2}\left(\frac{a}{b}\right)^{3/2}$$

$$\sqrt{\frac{\pi\left(\frac{ka}{2}\right)^{1/3}\theta^2}{i\sin\theta}}\ \frac{e^{i\pi/4}}{i}\left(\frac{2}{ka}\right)^{1/3}(2\pi)^{1/2} D_E(-\beta_1, -\beta_2)$$

$$\frac{e^{-ix_2 t_2}}{t_2 - q_2^2}\ \frac{e^{-ix_1 t_1}}{t_1 - q_1^2}\ \frac{w_1(t_2 - y_b)}{w_1(t_2)}\ \frac{w_1(t_1 - y)}{w_1(t_1)}\ , \tag{4.6}$$

where x_2 and x_1 are defined in Appendix C.

I will make more approximations after calculating the edge-diffraction coefficient in Section 5.

5. EDGE-DIFFRACTION COEFFICIENT FOR A LAND-SEA INTERFACE

Figure 6 shows the geometry for edge diffraction by a plane interface in which the surface impedance changes discontinuously as it does at a land-sea interface. Let u_i be the incident field at the land-sea interface that would exist if there were free space everywhere. Let u_d be the diffracted field a distance ℓ from the land-sea interface. Let

$$R_2 = \frac{\sin\beta_2 + \Delta_2}{\sin\beta_2 - \Delta_2} \tag{5.1}$$

be the Fresnel reflection coefficient for reflection of the incident wave at an angle of incidence $\pi/2 - \beta_2$ from Medium 2. Let

$$R_1 = \frac{\sin\beta_1 + \Delta_1}{\sin\beta_1 - \Delta_1} \tag{5.2}$$

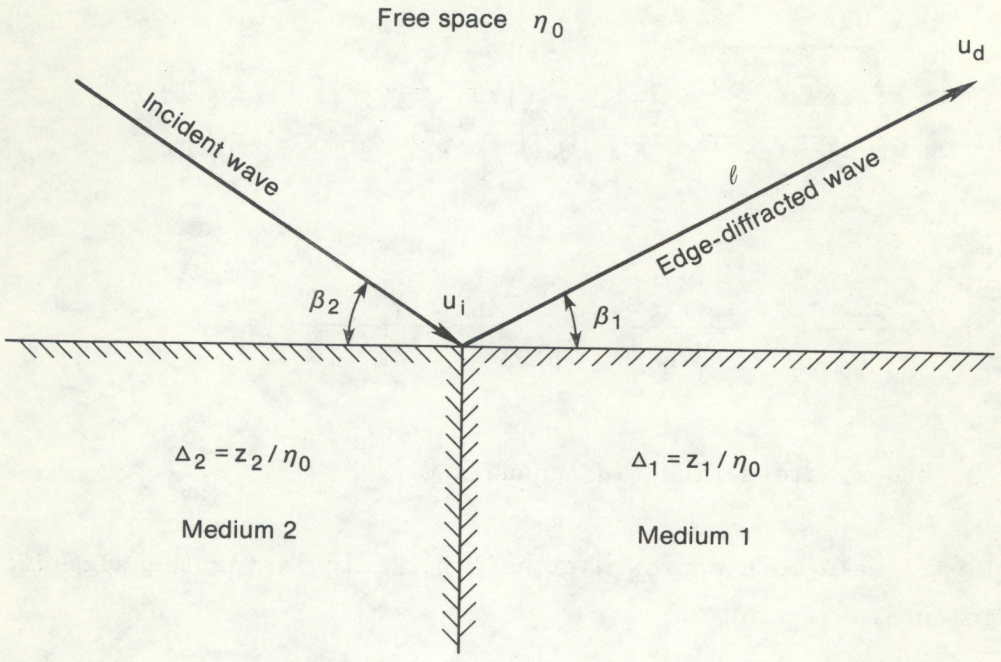

Figure 6. Geometry for edge diffraction at a land-sea interface. Each of the two lower media is characterized by a surface impedance z_2 or z_1. We consider a plane wave to be incident on the land-sea interface. One ray of the cylindrical edge-diffracted wave is shown.

be the Fresnel reflection coefficient for reflection of a wave at the angle β_1 from Medium 1. Δ_1, Δ_2, β_1, and β_2 are defined in Fig. 6.

The incident wave u_i gives rise to a diffracted wave

$$u_i D_E(\beta_1,\beta_2) \frac{e^{-ik\ell}}{\sqrt{k\ell}} ,$$

in the direction β_1 and a diffracted wave

$$u_i D_E(-\beta_1,\beta_2) \frac{e^{-ik\ell}}{\sqrt{k\ell}} ,$$

in the direction $-\beta_1$. The latter gets reflected into the β_1 direction to give a diffracted wave

$$u_i D_E(-\beta_1,\beta_2)\, R_1 \frac{e^{-ik\ell}}{\sqrt{k\ell}} .$$

The incident wave also gets reflected to produce a wave

$$u_i R_2 ,$$

from the $-\beta_2$ direction. This reflected wave in turn generates two diffracted waves,

$$u_i R_2 D_E(\beta_1,-\beta_2) \frac{e^{-ik\ell}}{\sqrt{k\ell}}$$

and

$$u_i R_2 D_E(-\beta_1,-\beta_2)\, R_1 \frac{e^{-ik\ell}}{\sqrt{k\ell}} ,$$

in the β_1 direction. Thus, there are four contributions to the diffracted wave u_d. Adding them together gives

$$u_d = u_i[D_E(\beta_1,\beta_2) + R_1 D_E(-\beta_1,\beta_2) + R_2 D_E(\beta_1,-\beta_2)$$

$$+ R_1 R_2 D_E(-\beta_1,-\beta_2)] \frac{e^{-ik\ell}}{\sqrt{k\ell}} . \tag{5.3}$$

Kaminetzky and Keller (1972) calculated the diffracted field for the geometry of Fig. 6. Their result [from their Equations (1.6) and (1.7) specialized to the case j=1] in the present notation is

$$u_d = \frac{u_i (2/\pi)^{1/2} e^{-i\pi/4} \sin\beta_1 \sin\beta_2 (\Delta_2-\Delta_1)}{(\sin\beta_2-\Delta_2)(\sin\beta_1-\Delta_1)(\cos\beta_2-\cos\beta_1)} \frac{e^{-ik\ell}}{\sqrt{k\ell}} . \tag{5.4}$$

Using (5.1) and (5.2), we can write (5.4) as

$$u_d = u_i (2/\pi)^{1/2} e^{-i\pi/4} \frac{(1+R_1)(1+R_2)}{4} \frac{\Delta_2-\Delta_1}{\cos\beta_2-\cos\beta_1} \frac{e^{-ik\ell}}{\sqrt{k\ell}} . \tag{5.5}$$

Comparing (5.3) with (5.5), we see that they are the same if we take

$$D_E(\beta_1,\beta_2) = \frac{e^{-i\pi/4}}{2(2\pi)^{1/2}} \frac{\Delta_2-\Delta_1}{\cos\beta_2-\cos\beta_1} . \tag{5.6}$$

We see that D_E is even in both of its arguments. Thus, we can write (5.3) as

$$u_d = u_i (1 + R_1)(1 + R_2) D_E (\beta_1,\beta_2) \frac{e^{-ik\ell}}{\sqrt{k\ell}} . \tag{5.7}$$

The above development requires a little comment. First, I altered (5.4) slightly from the original formula given by Kaminetzky and Keller. Their result was valid only for

$$|\Delta_2-\Delta_1| << |\Delta_1| \tilde{} |\Delta_2| , \tag{5.8}$$

and they made no distinction between Δ_1 and Δ_2 in the denominator of (5.4). Within the limitations of (5.8), (5.4) is equivalent to the expression given by Kaminetzky and Keller. However, the agreement of (5.4) with the formulas of Hill and Wait (1981), which we shall see later, indicates that (5.4) may be valid without the restriction (5.8).

Second, I included the reflection coefficients R_1 and R_2 in (5.7) but did not include them in the 6th factor in (4.1), because in (4.1) the wave incident on the land-sea interface was a surface-diffracted wave (i.e., a creeping ray or groundwave). A groundwave already has a reflection coefficient included in it. In fact, the expansion in a groundwave mode series is a residue expansion at the poles of the ground reflection coefficient. A ground reflection coefficient is already included in both the groundwave incident on the land-sea interface and the groundwave excited at the interface. Because groundwaves occur where the reflection coefficient has a pole, we have

$$|R_1| >> 1 \tag{5.9}$$

and

$$|R_2| >> 1 \tag{5.10}$$

for groundwaves, so that (5.7) becomes

$$u_d = u_i R_1 R_2 D_E(\beta_1, \beta_2) \frac{e^{-ik\ell}}{\sqrt{k\ell}} \quad , \tag{5.11}$$

where $R_1 R_2$ is already included in the groundwaves.

We can consider some other forms for (5.6). If the wave incident on the land-sea interface is a groundwave, and if the edge-diffracted wave is a groundwave, then (A.6) and (A.7) give the incident and diffracted angles. Substituting (A.6) and (A.7) into (5.6) gives

$$D_E = \left(\frac{ka}{2}\right) \frac{e^{-i\pi/4}}{(2\pi)^{1/2}} \frac{\Delta_1-\Delta_2}{\nu_1-\nu_2} . \tag{5.12}$$

Using (B.3) through (B.6) in (5.12) gives

$$D_E = i\left(\frac{ka}{2}\right)^{1/3} \frac{e^{-i\pi/4}}{(2\pi)^{1/2}} \frac{q_1-q_2}{t_1-t_2} . \tag{5.13}$$

Another special case arises if the incident wave on the land-sea interface is a groundwave but the edge-diffracted ray is scattered at some arbitrary angle β_1. Then we can use (A.6), (B.3), (B.5), and (B.6) in (5.6) to get

$$D_E = i(ka/2)^{1/3} \frac{e^{-i\pi/4}}{(2\pi)^{1/2}} \frac{q_1-q_2}{t_{eff}-t_2} , \tag{5.14}$$

where

$$t_{eff} \equiv 2(ka/2)^{2/3}(\cos\beta-1) , \tag{5.15}$$

and I have written the scattering angle as β instead of β_1.

6. COMPARISON WITH THE FORMULAS OF HILL AND WAIT

Hill and Wait (1981) calculate groundwave-mode coupling at the land-sea interface. It is appropriate, therefore, to compare (4.6) with their formula. The appropriate edge-diffraction coefficient D_E is given by (5.13), because it corresponds to both the incident and edge-diffracted waves being groundwave modes. Substituting (5.13) into (4.6) gives

$$E/E_o = \left[\sqrt{2}\left(\frac{ka}{2}\right)^{1/3}\left(\frac{y_b - t_2}{k^2b^2 - \nu_2^2}\right)^{1/4}\right]\left[\sqrt{2}\left(\frac{ka}{2}\right)^{1/3}\left(\frac{y - t_1}{k^2r^2 - \nu_1^2}\right)^{1/4}\right]\left(\frac{a}{r}\right)^{3/2}\left(\frac{a}{b}\right)^{3/2}$$

$$\sqrt{\frac{\pi\left(\frac{ka}{2}\right)^{1/3}\theta^2}{i\sin\theta}}\left(\frac{q_1 - q_2}{t_1 - t_2}\right)$$

$$\frac{e^{-ix_2t_2}}{t_2 - q_2^2}\;\frac{e^{-ix_1t_1}}{t_1 - q_1^2}\;\frac{w_1(t_2 - y_b)}{w_1(t_2)}\;\frac{w_1(t_1 - y)}{w_1(t_1)} \quad . \tag{6.1}$$

Equation (6.1) is valid for arbitrary source and observer heights. If the source and observer are close to the surface of the Earth, such that the angles β_T and β_R (Fig. 5) are small, then

$$b \tilde{\sim} r \tilde{\sim} a, \tag{6.2}$$

(B.1) is approximately

$$t_2 - y_b \tilde{\sim} \left(\frac{2}{ka}\right)^{1/3}(ka + \left(\frac{ka}{2}\right)^{1/3} t_2 - kb) = t_2 - (2/ka)^{1/3}kh_b, \tag{6.3}$$

(B.2) is approximately

$$t_1 - y \tilde{\sim} \left(\frac{2}{ka}\right)^{1/3}(ka + \left(\frac{ka}{2}\right)^{1/3} t_1 - kr) = t_1 - (2/ka)^{1/3}kh, \tag{6.4}$$

and the two factors in square brackets in (6.1) are both unity.

With these approximations, (6.1) becomes

$$E/E_o = \sqrt{\frac{\pi(ka/2)^{1/3}\theta^2}{i\sin\theta}}\ \frac{q_1-q_2}{t_1-t_2}\ \frac{e^{-ix_2t_2}}{t_2-q_2^2}\ \frac{e^{-ix_1t_1}}{t_1-q_1^2}$$

$$\frac{w_1(t_2-y_b)}{w_1(t_2)}\ \frac{w_1(t_1-y)}{w_1(t_1)}\ , \tag{6.5}$$

where, from (6.3)

$$y_b = (2/ka)^{1/3}kh_b\ , \tag{6.6}$$

and from (6.4)

$$y = (2/ka)^{1/3}kh. \tag{6.7}$$

One further approximation can often be made if the horizontal distance between the source and observer are small enough that

$$\sin\theta \tilde{\sim} \theta\ . \tag{6.8}$$

Then (6.5) becomes

$$E/E_o = (\pi x/i)^{1/2}\ \frac{(q_1-q_2)\ \exp(-ix_2t_2-ix_1t_1)}{(t_1-t_2)(t_2-q_2^2)(t_1-q_1^2)}\ \frac{w_1(t_2-y_b)}{w_1(t_2)}\ \frac{w_1(t_1-y)}{w_1(t_1)}\ , \tag{6.9}$$

where x is defined in (C.3). Of course, (6.9) gives the effect of only one groundwave mode from the sea exciting only one land-type groundwave mode at the land-sea interface. The total field is found by summing over all sea-type and land-type groundwave modes.

$$E_{tot}/E_o = (\pi x/i)^{1/2}(q_1-q_2)\sum_{t_1}\sum_{t_2}\frac{\exp(-ix_2t_2-ix_1t_1)}{(t_1-t_2)(t_2-q_2^2)(t_1-q_1^2)}\ \frac{w_1(t_2-y_b)}{w_1(t_2)}\ \frac{w_1(t_1-y)}{w_1(t_1)}\ . \tag{6.10}$$

Equation (6.10) agrees with the corresponding formula of Hill and Wait (1981; Eq. 9).

The agreement indicates that edge-diffraction is probably the mechanism for coupling of groundwave modes at a land-sea interface.

7. THE DIRECT EDGE-DIFFRACTED WAVE NEAR THE LAND-SEA INTERFACE

Now that we know that edge-diffraction is the mechanism for coupling groundwaves at a land-sea interface, we see that groundwaves incident on such a land-sea interface will excite edge-diffracted waves in all directions, and that it might be possible to detect such waves near the shoreline. Figure 7 shows the geometry that allows the calculation of these edge-diffracted waves. It is similar to Fig. 5 in that the creeping ray (the caustic for the surface-diffracted ray) is shown unrealistically below the Earth, so that the ray from the caustic to the land-sea interface can be shown tangent to the caustic.

Following the example in Section 4, we can calculate the vertical electric field, seen by the observer in Fig. 7, due to a vertical electric dipole source. This is

$$E = \left[i \frac{Ids\omega\mu_o}{4\pi} \frac{e^{-ik\ell_T}}{\ell_T} \cos\beta_T \right] \left[D_{\nu_2}(\ell_T) \right] \left[e^{-i\nu_2\alpha_2} \right] \left[S_{\nu_2}(\ell_2) \right]$$

$$\left[e^{-ik\ell_2} \right] \left[D_E(\beta, -\beta_2) \right] [1 + R_1] \left[\frac{1}{\sqrt{k\ell}} \right] \left[e^{-ik\ell} \right] \left[\sqrt{\frac{\frac{\nu_2}{k} \sin\beta_T}{r \sin\theta}} \right] [\sin\phi]. \quad (7.1)$$

The 11 factors in (7.1) are respectively

1) The incident field from the vertical electric dipole source at the point of excitation of the sea-type groundwave.

2) The groundwave excitation coefficient.

3) The phase integral of the surface-diffracted ray from the point of excitation to the point of shedding.

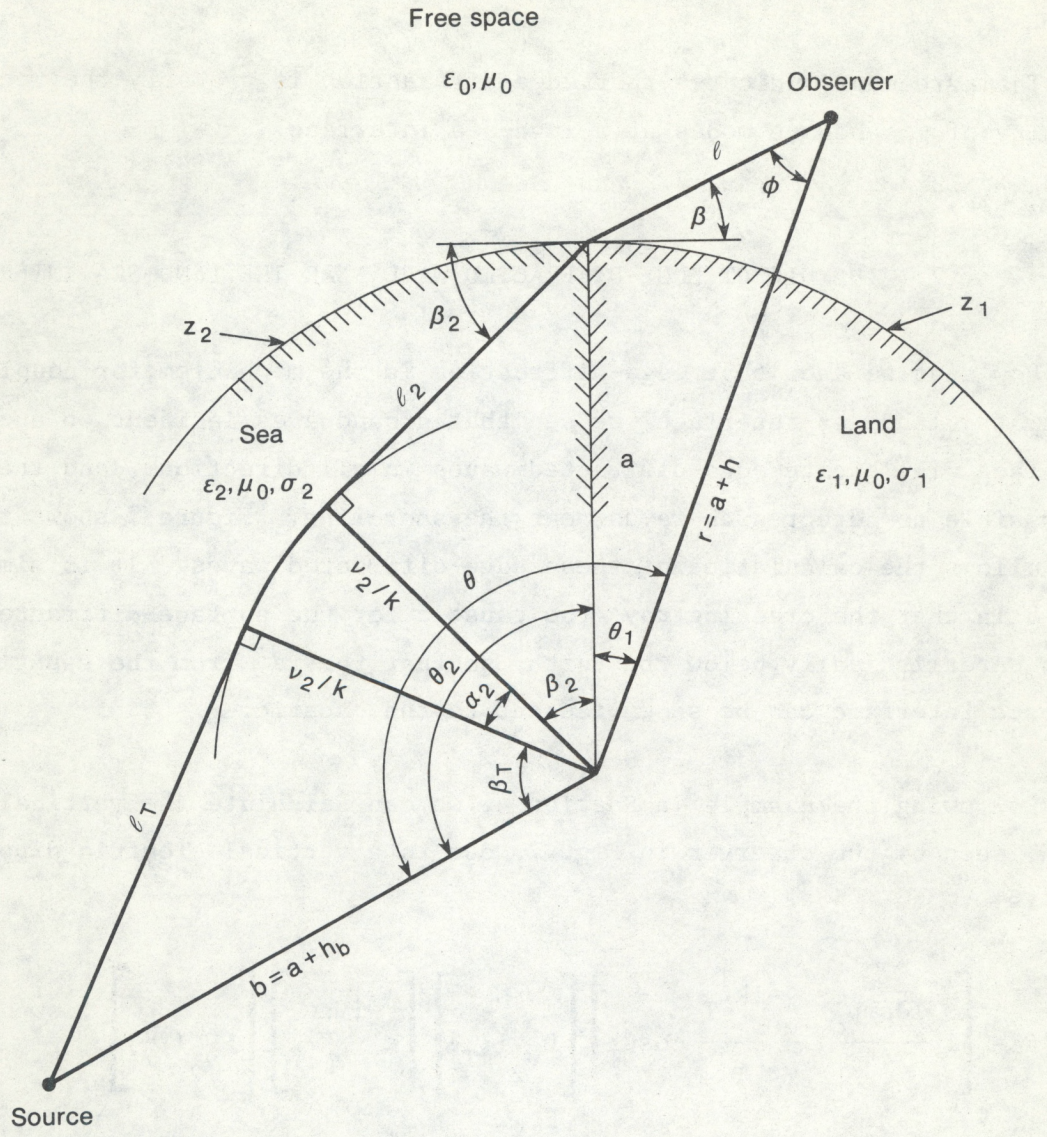

Figure 7. Geometry to represent excitation of an edge-diffracted wave by a groundwave mode incident on a land-sea boundary. One ray of the cylindrical edge-diffracted wave is shown.

4) The shedding coefficient.

5) The phase integral from the point of shedding to the land-sea interface.

6) The edge-diffraction coefficient for an incident grazing angle $-\beta_2$ and a scattering angle β.

7) One plus the ground reflection coefficient for the land.

8) The geometrical spreading factor for the cylindrical wave scattering from the land-sea interface.

9) The phase integral from the land-sea interface to the observer.

10) A covergence factor to account for azimuthal focusing.

11) The pattern factor of the receiving antenna (a vertical dipole).

Equation (7.1) can be written in terms of known quantities by using the geometrical relationships in Fig. 7 (given in Appendix A), the groundwave excitation and shedding coefficients in Table 1 (with auxiliary formulas given explicitly for the geometry of Fig. 7 in Appendix B), and the appropriate form for the edge-diffraction coefficient (5.14). The result (after some algebra) is

$$E = \left[\sqrt{2}\left(\frac{ka}{2}\right)^{1/3}\left(\frac{y_b - t_2}{k^2b^2 - \nu_2^2}\right)^{1/4}\right]\left[\sqrt{2}\left(\frac{ka}{2}\right)^{1/3}\left(\frac{-t_2}{k^2a^2 - \nu_2^2}\right)^{1/4}\right]\left(\frac{\nu_2}{kb}\right)^{3/2}\left(\frac{a}{r}\right)^{1/2}$$

$$\frac{1}{2}\left(2i\,\frac{Ids\omega\mu_o}{4\pi a\theta}\right)\left(\frac{ka\theta^2}{\sin\theta}\right)^{1/2}\frac{q_1 - q_2}{t_{eff} - t_2}\,\frac{e^{-i\nu_2\theta_2}}{t_2 - q_2^2}\,\frac{w_1(t_2 - y_b)}{w_1(t_2)}$$

$$\frac{2i}{w_1(t_1)w_2(t_1)(w_1'(t_1)/w_1(t_1) - q_1)}\,\frac{e^{-ik\ell}}{\sqrt{k\ell}}\sin\phi, \qquad (7.2)$$

where I have used

$$R_1 = -\frac{w_2'(t_1)/w_2(t_1) - q_1}{w_1'(t_1)/w_1(t_1) - q_1} \tag{7.3}$$

for the ground reflection coefficient, and the Wronskian

$$w_1(t)w_2'(t) - w_2(t)w_1'(t) = -2i. \tag{7.4}$$

As in Section 4, when (4.3) holds, the second factor in square brackets is unity. In addition, if we use (4.3) nearly everywhere but in exponential terms, and divide by (4.5), we get

$$E/E_o = \left[\sqrt{2}\left(\frac{ka}{2}\right)^{1/3}\left(\frac{y_b - t_2}{k^2b^2 - \nu_2^2}\right)^{1/4}\right]\left(\frac{a}{b}\right)^{3/2}\left(\frac{a}{r}\right)^{1/2}\frac{1}{2}\left(\frac{ka\theta^2}{\sin\theta}\right)^{1/2}$$

$$\frac{2i}{w_1(t_1)w_2(t_1)(w_1'(t_1)/w_1(t_1) - q_1)}$$

$$\frac{q_1 - q_2}{t_{eff} - t_2}\;\frac{e^{-ix_2t_2}}{t_2 - q_2^2}\;\frac{w_1(t_2 - y_b)}{w_1(t_2)}\;\frac{e^{-ik\ell + ika\theta_1}}{(k\ell)^{1/2}}\sin\phi. \tag{7.5}$$

As in Section 6, if the source and observer are close enough to the ground (within about 100 km) then the factor in square brackets is approximately unity. In addition, we can use (6.2) in (7.5) to give

$$E/E_o = \frac{1}{2}\left(\frac{ka\theta^2}{\sin\theta}\right)^{1/2}\frac{q_1 - q_2}{t_{eff} - t_2}\;\frac{e^{-ix_2t_2}}{t_2 - q_2^2}\;\frac{w_1(t_2 - y_b)}{w_1(t_2)}\;\frac{e^{-ik\ell + ika\theta_1}}{(k\ell)^{1/2}}\sin\phi$$

$$\frac{2i}{w_1(t_1)w_2(t_1)(w_1'(t_1)/w_1(t_1) - q_1)}\,. \tag{7.6}$$

Further, if the source-observer distance is not too large, we can use (6.8) in (7.6) to give

$$E/E_o = \frac{1}{2}(ka\theta)^{1/2} \frac{q_1-q_2}{t_{eff}-t_2} \frac{e^{-ix_2t_2}}{t_2-q_2^2} \frac{w_1(t_2-y_b)}{w_1(t_2)} \frac{e^{-ik\ell+ika\theta_1}}{(k\ell)^{1/2}} \sin\phi$$

$$\frac{2i}{w_1(t_1)w_2(t_1)(w_1'(t_1)/w_1(t_1) - q_1)} . \tag{7.7}$$

The formulas presented here are not valid near the horizon because of surface diffraction effects (excitation of groundwaves). I tried to extend the validity of the results by writing the field as a contour integral that I could evaluate by a saddlepoint approximation to get the formulas presented here. Near the horizon, however, the saddlepoint was near a pole and near an endpoint in the contour integration. Because of that and other difficulties, I was not able to extend the validity of these formulas closer to the horizon. Although a different contour integral representation might work, it is not of great importance to do this because the groundwave mode representation works well near the horizon.

8. DIRECT RECEPTION OF A SEA-TYPE GROUNDWAVE OVER THE LAND

Figure 8 shows how it is possible to receive directly a sea-type groundwave over the land. If the frequency is high enough, then the possible edge effect from the land-sea interface will be negligible. The point is that the presence of the land in Fig. 8 should not be significant because the ray does not touch the land. The signal seen by the observer should be nearly the same as that for the case of a homogeneous sea.

The condition that the observer is close enough to the land-sea interface so that the situation in Fig. 8 applies is

$$\theta_1 < \cos^{-1}\frac{\nu_2}{kr} - \cos^{-1}\frac{\nu_2}{ka} . \tag{8.1}$$

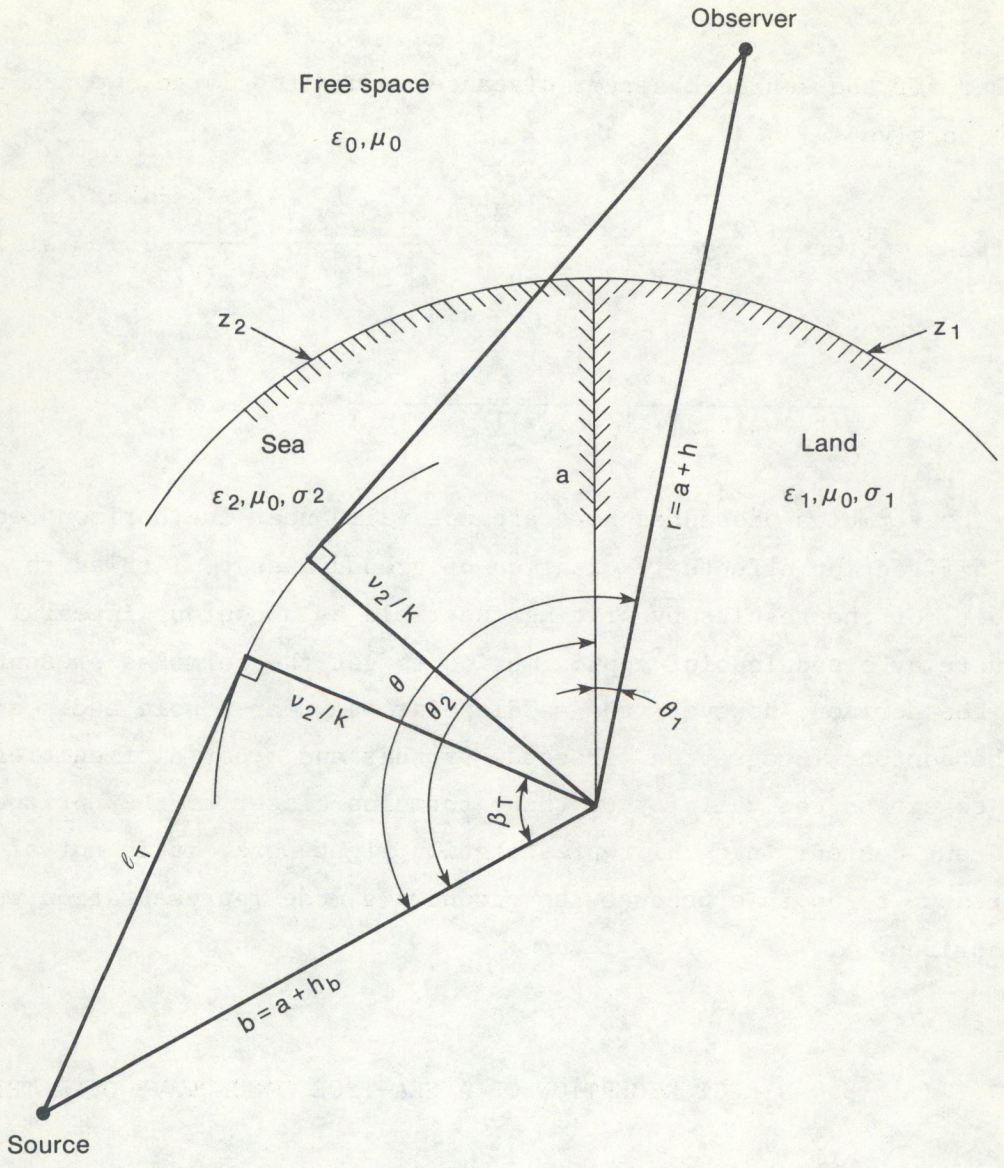

Figure 8. Geometry showing how a sea-type groundwave mode can be observed over land by an elevated observer.

In Fig. 8, the radius ν_2/k of the caustic associated with the surface-diffracted wave is represented as being real. Normally, however, ν_2 is complex, so that the radius ν_2/k is also complex and the angles in (8.1) are also complex. Thus, in general, it may be appropriate to substitute

$$\theta_1 < \text{real} \left(\cos^{-1} \frac{\nu_2}{kr} - \cos^{-1} \frac{\nu_2}{ka} \right) \tag{8.2}$$

for (8.1). I admit that this is an ad hoc procedure. However, it seems to have about the right properties and can probably be justified with more careful analysis. If the angles in (8.2) are small (as they usually are) then (8.2) may be approximated by

$$x_1 < \text{real} \left(\sqrt{y - t_2} - \sqrt{-t_2} \right), \tag{8.3}$$

where x_1 is defined in (C.2), y is defined in (6.7), and t_2 is related to ν_2 by (B.3) and is defined as one of the roots of (B.7).

In practice, as θ_1 (or x_1) increases, the higher order groundwave modes will cease to satisfy (8.3) first and be cut off. As θ_1 (or x_1) continues to increase, more and more of the high order modes will be cut off until only the lowest order mode exists, and then finally it too will be cut off as θ_1 (or x_1) continues to increase.

The higher the observer (the larger y is) the larger θ_1 (or x_1) will be for cut off of a given groundwave mode. When the observer is on the ground, all groundwave modes are cut off beyond the land-sea interface.

Figure 9 shows the cut-off situation for which (8.2) or (8.3) is not satisfied.

9. THE SHADOW ZONE FOR A GROUNDWAVE MODE EXCITED AT A LAND-SEA INTERFACE

Figure 10 shows an observer over the land receiving a land-type groundwave mode. As pointed out in Section 3, a groundwave mode is a ground-reflected wave

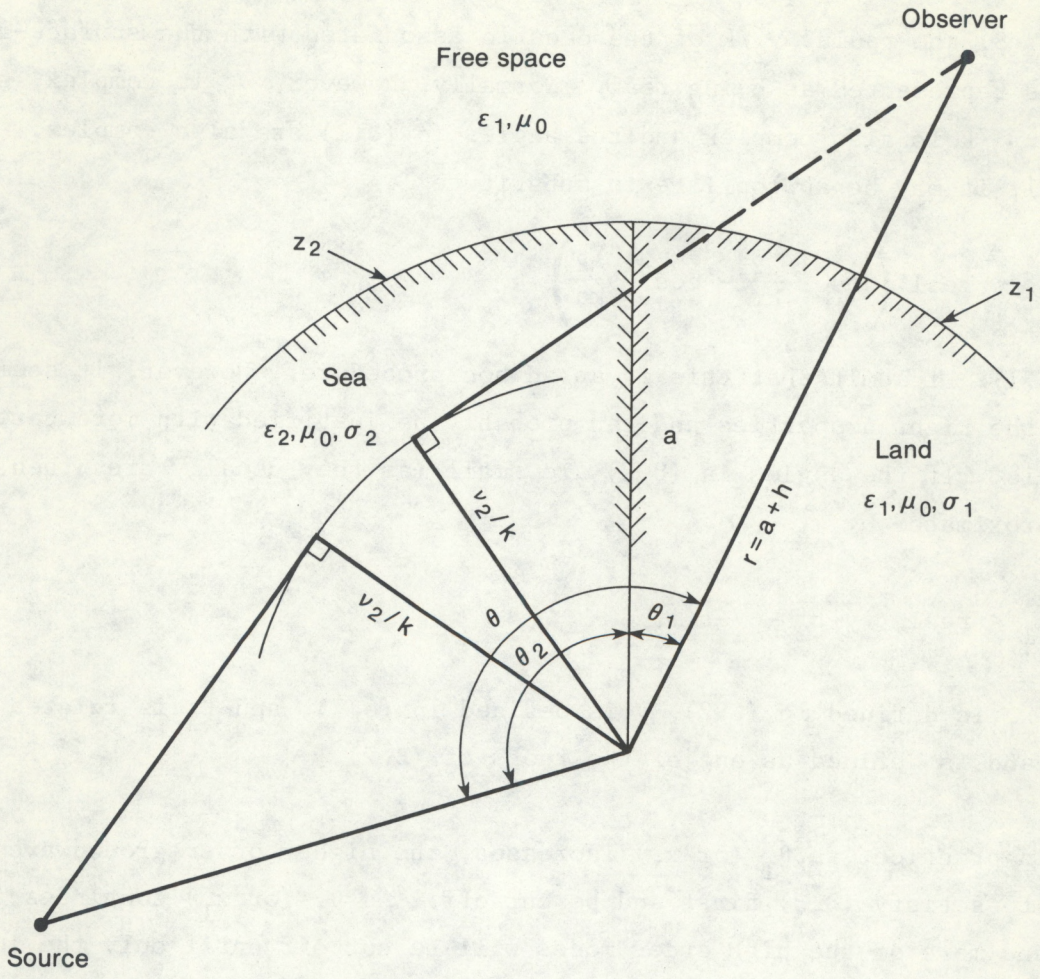

Figure 9. Geometry showing cut off of a sea-type groundwave mode for an elevated observer who is too far from the shoreline.

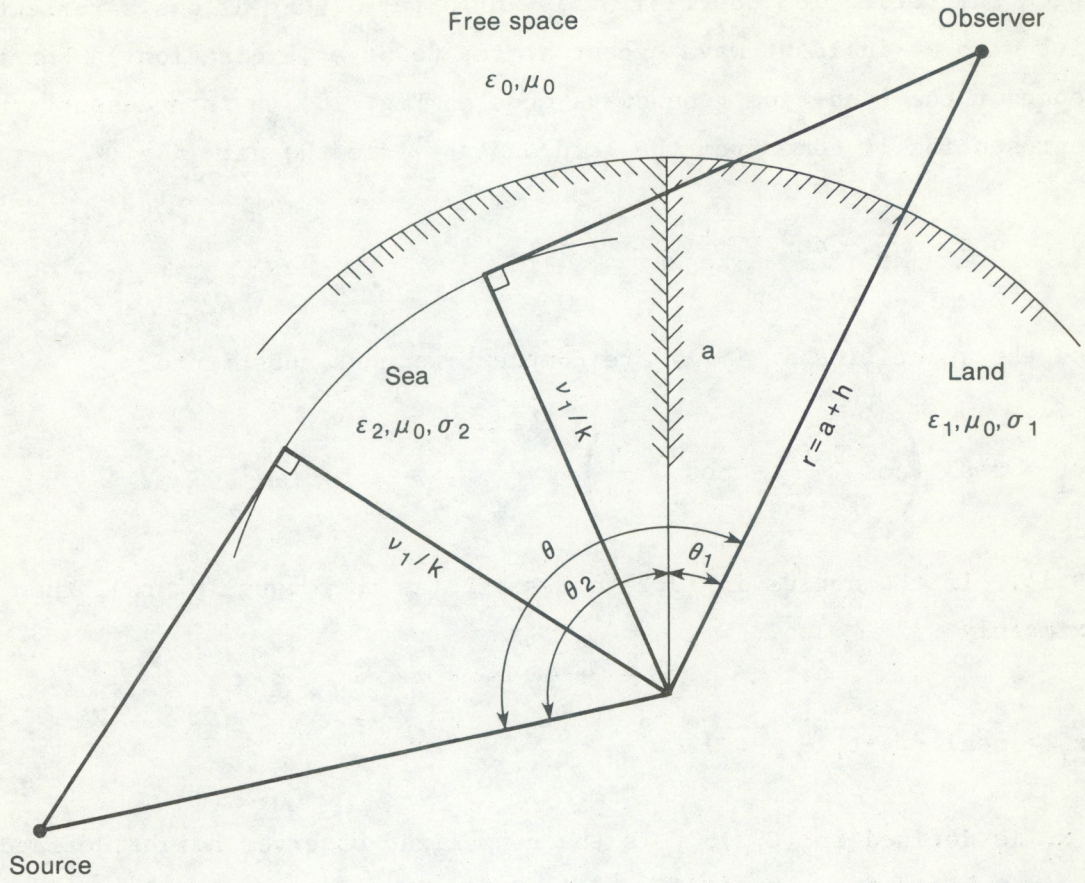

Figure 10. Geometry showing how the ray that represents a land-type groundwave mode propagates in a straight line from the Earth's surface to the observer. The ray must intersect the Earth's surface on the land side of the land-sea interface to satisfy the boundary condition (an infinite ground reflection coefficient) for a land-type groundwave mode.

for which the reflection coefficient is infinite. (That allows a reflected wave to exist with no incident wave except at the point of excitation.) For the existence of the land-type groundwave mode in Fig. 10, it is necessary that the ray representing it come from the land and not from the sea; i.e.,

$$\theta_1 > \cos^{-1}\frac{\nu_1}{kr} - \cos^{-1}\frac{\nu_1}{ka} . \tag{9.1}$$

Because the quantities in (9.1) are complex, we must substitute

$$\theta_1 > \text{real}\left(\cos^{-1}\frac{\nu_1}{kr} - \cos^{-1}\frac{\nu_1}{ka}\right) \tag{9.2}$$

for (9.1). If the angles in (9.2) are small (as they usually are), then (9.2) is approximately

$$x_1 > \text{real}\,(\sqrt{y-t_1} - \sqrt{-t_1}), \tag{9.3}$$

where x_1 is defined in (C.2), y is the normalized observer height defined in (6.7), and t_1 is related to ν_1 by (B.4) and is defined as one of the roots of (B.8).

Figure 11 shows the opposite case, where (9.2) and (9.3) do not hold. The land-type groundwave mode seen by the observer in Fig. 11 appears to come from the sea. It is clear that the physical conditions necessary (an infinite reflection coefficient) for the existence of that groundwave mode do not hold there. It therefore seems likely that (9.3) is approximately a correct condition for the observation of the groundwave mode in question. There thus seems to be a shadow zone for each land-type groundwave mode. The observer in Fig. 11 is in the shadow zone for the groundwave mode represented, whereas the observer in Fig. 10 is not in the shadow zone.

In practice, an observer directly above the land-sea interface is in the shadow zone for all of the land-type groundwave modes that have been excited at the land-sea interface. As the observer moves over land, he moves out of the shadow zone of the higher order modes. If he moves far enough away from the sea, he will move out of the shadow zone of all of the land-type groundwave modes.

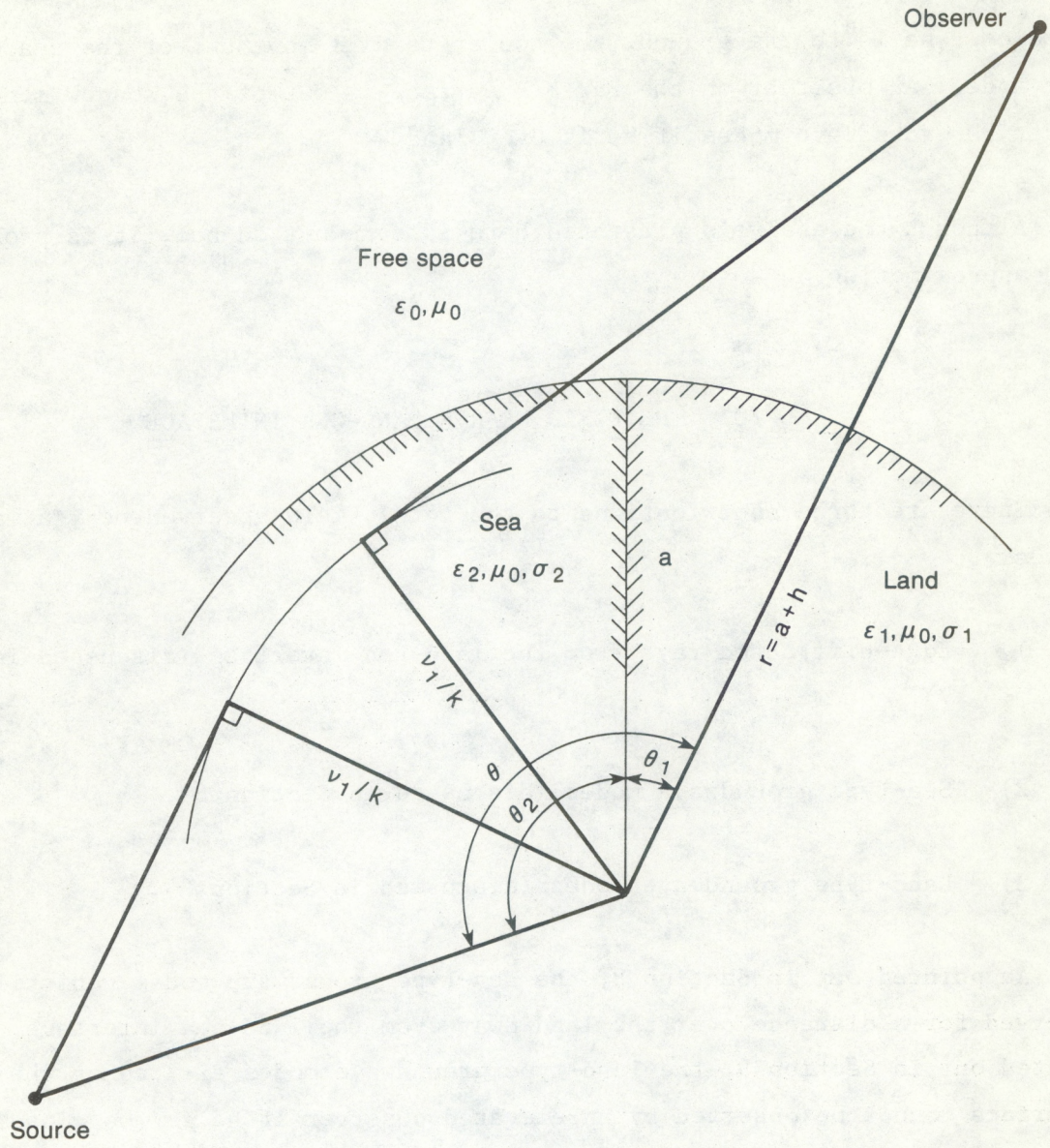

Figure 11. Geometry for an observer in the shadow zone of the land-type groundwave mode that was excited at the land-sea interface. The ray that would connect the caustic of the land-type groundwave mode with the observer intersects the Earth's surface over the sea. At that point of intersection, the ray fails to satisfy the boundary condition (an infinite ground reflection coefficient).

The closer he is to the ground, the sooner he will move out of the shadow zone of each mode. An observer on the Earth's surface is out of the shadow zone of all land-type groundwave modes if he is over land.

Although the analysis presented here is somewhat ad hoc, it is probably a good approximation.

10. THE FIELD NEAR A LAND-SEA INTERFACE

There are three contributions to the total field observed near a land-sea boundary.

1) Edge-diffracted rays from the land-sea interface (discussed in Section 7).

2) Sea-type groundwave modes (discussed in Section 8).

3) Land-type groundwave modes (discussed in Section 9).

As pointed out in Section 8, the sea-type groundwave modes can still be observed for a distance over the land away from the land-sea interface. As pointed out in Section 9, the land-type groundwave modes excited at the land-sea interface cannot be observed by an elevated observer if he is too close to the land-sea interface. Thus, the significant variation of the groundwave mode contributions to the field is determined by the number of contributing modes for each of the two types.

Figure 12 shows a plot of these three contributions for an observer 30 m above the ground [relative to the free-space field above a flat, perfect conductor (4.5)]. The edge-diffracted wave is very small near the land-sea interface, and increases as the observer moves away from the sea. The main cause of the rapid increase is the factor $t_{eff}-t_2$ in the denominator of (7.5). t_2 is small and complex with a postiive real part. As can be seen from (5.15), t_{eff} is real and negative. The denominator $t_{eff}-t_2$ will be smallest for small

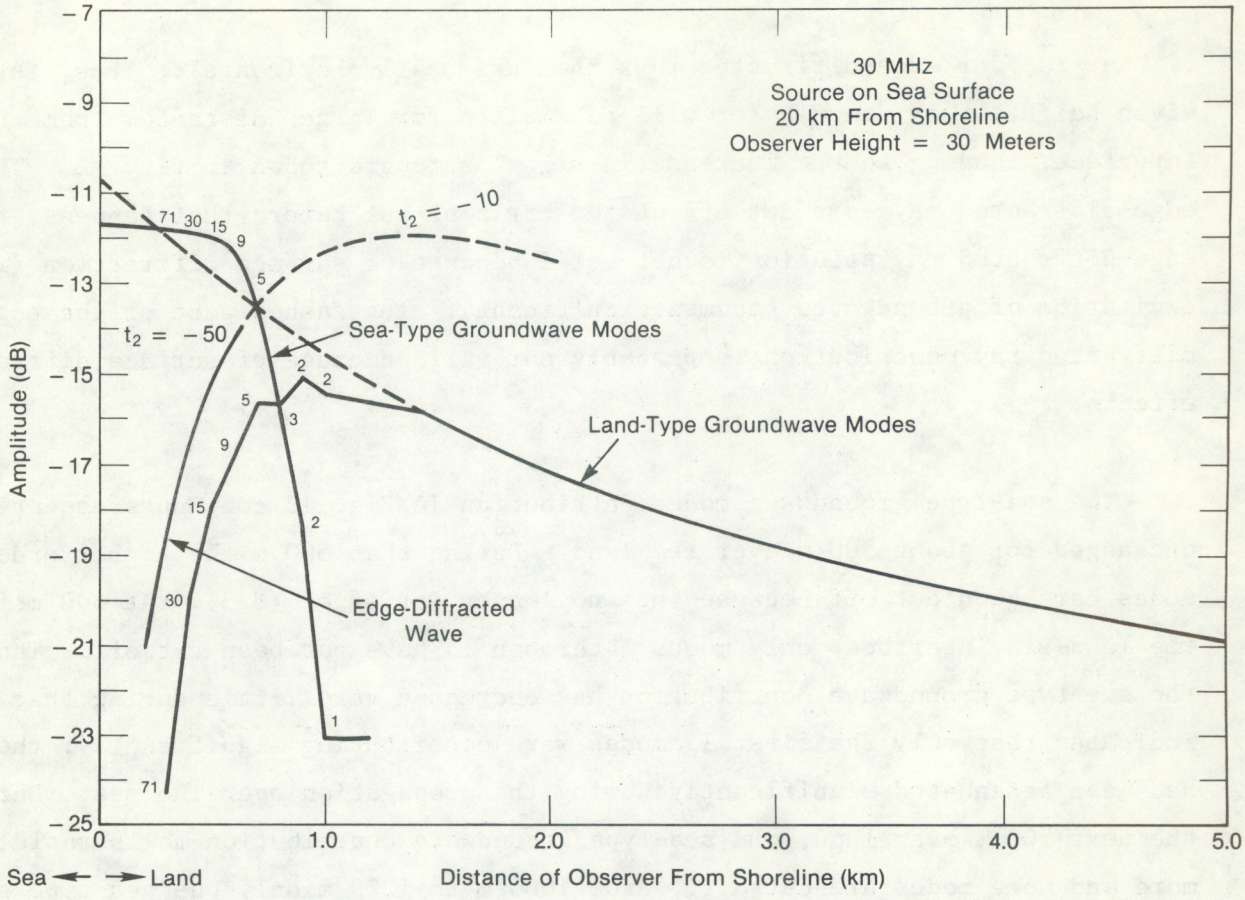

Figure 12. The field (relative to the free-space field above a flat perfect conductor) near the land-sea interface for an observer 30 m above sea level. The source is a vertical electric dipole on the surface of the sea 20 km from the shoreline. The frequency is 30 MHz. The numbers near the sea-type groundwave-mode contribution indicate the maximum mode number included in the calculation. The numbers near the land-type groundwave-mode contribution indicate the maximum mode number not included in the calculation. A maximum of 200 modes were used in these calculations. The dashed-line extension to the land-type groundwave-mode contribution indicates the sum of the first 200 modes. The dashed-line portion of the edge-diffracted wave indicates the region where the approximations used to calculate the edge-diffracted wave are no longer valid because surface diffraction by the Earth is significant. The values of t_2 used in (7.7) are given on the curve for the edge-diffracted wave. Large negative values for t_2 (such as -50) indicate that the effect of surface diffraction by the Earth is not significant. Because the edge-diffracted wave and the land-type groundwaves are alternate representations of the same field, the correct contribution to that part of the field will follow the edge-diffracted wave near the land-sea interface and the land-type groundwave far from the land-sea interface. The total field is found by summing (coherently) the sea-type groundwave with the edge-diffracted/land-type groundwave contribution.

β, that is, for edge-diffracted rays that are nearly horizontal. Thus, for a given height, that denominator will be smaller for larger distances from the interface, leading to the increase in signal strength shown in Fig. 12. The edge-diffracted rays are cut off at the horizon, but before that happens, the edge-diffracted ray solution is not valid because of surface diffraction (i.e., excitation of groundwaves becomes significant). The dashed part of the edge-diffracted ray contribution is probably not valid because of surface diffraction effects.

The sea-type groundwave mode contribution in Fig. 12 continues essentially unchanged for about 500 m over the land. During that 500 m the higher order modes have been cut off because they no longer satisfied (8.3). At 500 m from the land-sea interface, only modes 1 through 15 have not been cut off. That the sea-type groundwave contribution has decreased very little during that 500 m indicates that only the first 15 modes were contributing significantly; the rest had been attenuated significantly during the propagation over the sea. During the next 500 m over land, the sea-type groundwave contribution falls rapidly as more and more modes are cut off. From 1000 m to 1200 m only one sea-type groundwave mode is not cut off. Beyond 1200 m all of the sea-type groundwave modes are cut off for an observer 30 m above the land. I suspect that a more thorough analysis would show the same qualitative behavior, but the distance from the shoreline where the rapid falloff occurs might be shifted a hundred meters or so.

The land-type groundwave mode contribution in Fig. 12 is negligible at the shoreline and grows as the observer moves farther inland and out of the shadow zone of more and more modes. The observer moves out of the shadow zone of the higher order modes first. Finally, at 1200 m from the shoreline the observer moves out of the shadow zone of the lowest order mode, and beyond that distance all of the land-type groundwave modes contribute. The contribution of all of the modes calculated (200) is shown with a dashed line for reference. Again, I suspect that a more thorough analysis would show the same qualitative behavior.

The agreement of the edge-diffracted ray contribution with the land-type groundwave mode contribution is significant. In fact, the two are not independent contributions, but rather alternate representations of the edge-diffracted contribution. The edge-diffracted ray is the more accurate representation

closer to the shoreline, while the groundwave mode representation is more accurate far from the shoreline.

The practical importance of Fig. 12 is that an observer 30 m above sea level can be as much as 500 m back from the shoreline before his received signal decreases significantly from what he would receive above the shoreline.

Figures 13 through 19 show similar behavior for observer heights varying from 10 m through 300 m. Figure 20 shows similar behavior for a source 70 km from the shoreline.

Figure 21 shows a contour plot in a vertical plane of the signal strength over the land for sea-to-land propagation. The three regions, the region where sea-type groundwaves are dominant, the transition region where some modes for both types of groundwaves are in the shadow, and the region where the land-type groundwaves are dominant are clearly shown. The exact shape of the contours in the transition region is uncertain because the exact transition of each groundwave mode across its shadow boundary was not calculated. The location of the transition region is reasonably accurate, however. Figures 22 and 23 show more details of the contours closer to the shoreline.

11. ACKNOWLEDGMENTS

I wish to thank David Hill of the Electromagnetics Division of the National Bureau of Standards for discussing some aspects of this problem with me and for the use of his program, MPHGAIN, which I modified to make the calculations. I thank T. M. Georges of the Wave Propagation Laboratory for suggesting this problem and for his comments after reading the manuscript. I thank the editorial staff of Publication Services for helping me clarify the expression of my ideas. I thank Joanne Shangle for her fast and accurate typing of the manuscript.

12. REFERENCES

Barrick, D. E., M. W. Evans, and B. L. Weber; Ocean surface currents mapped by radar, Science 198, 138-144, 1977.

Bremmer, H.; Terrestrial Radio Waves; Theory of Propagation, Elsevier, New York, 1949.

Hill, D. A. and J. R. Wait; HF ground wave propagation over mixed land, sea, and sea-ice paths, IEEE Trans. Geosci. Remote Sensing GE-19, pp. 210-216, 1981.

Jones, R. M.; Application of the geometrical theory of diffraction to terrestrial LF radio wave propagation, Mitteilungen aus dem Max-Planck-Institut für Aeronomie Nr. 37, Springer Verlag, Berlin, 1968.

Kaminetzky, L. and J. B. Keller; Diffraction coefficients for higher order edges and vertices, SIAM J. Appl. Math. 22, pp. 109-134, 1972.

Keller, J. B.; Geometrical theory of diffraction, J. Opt. Soc. Am. 52, No. 2, pp. 116-130, 1962.

Levy, B. R. and J. B. Keller; Diffraction by a smooth object, Commun. Pure. Appl. Math. 12, No. 1, pp. 159-209, 1959.

Wait, J. R.; Terrestrial propagation of VLF radio waves, J. Res. NBS 64D, No. 2, pp. 153-204, 1960.

Wait, J. R.; On the theory of mixed-path groundwave propagation on a spherical earth, J. Res. NBS 65D, pp. 401-410, 1961.

Wait, J. R. and L. C. Walters; Curves for ground wave propagation over mixed land and sea paths, IEEE Trans. Antennas Propagation. AP-11, pp. 38-45, 1963.

Watson, G. N.; The diffraction of electric waves by the earth, Proc. Royal Soc. London 95A, No. 666, pp. 83-99, October 7, 1918.

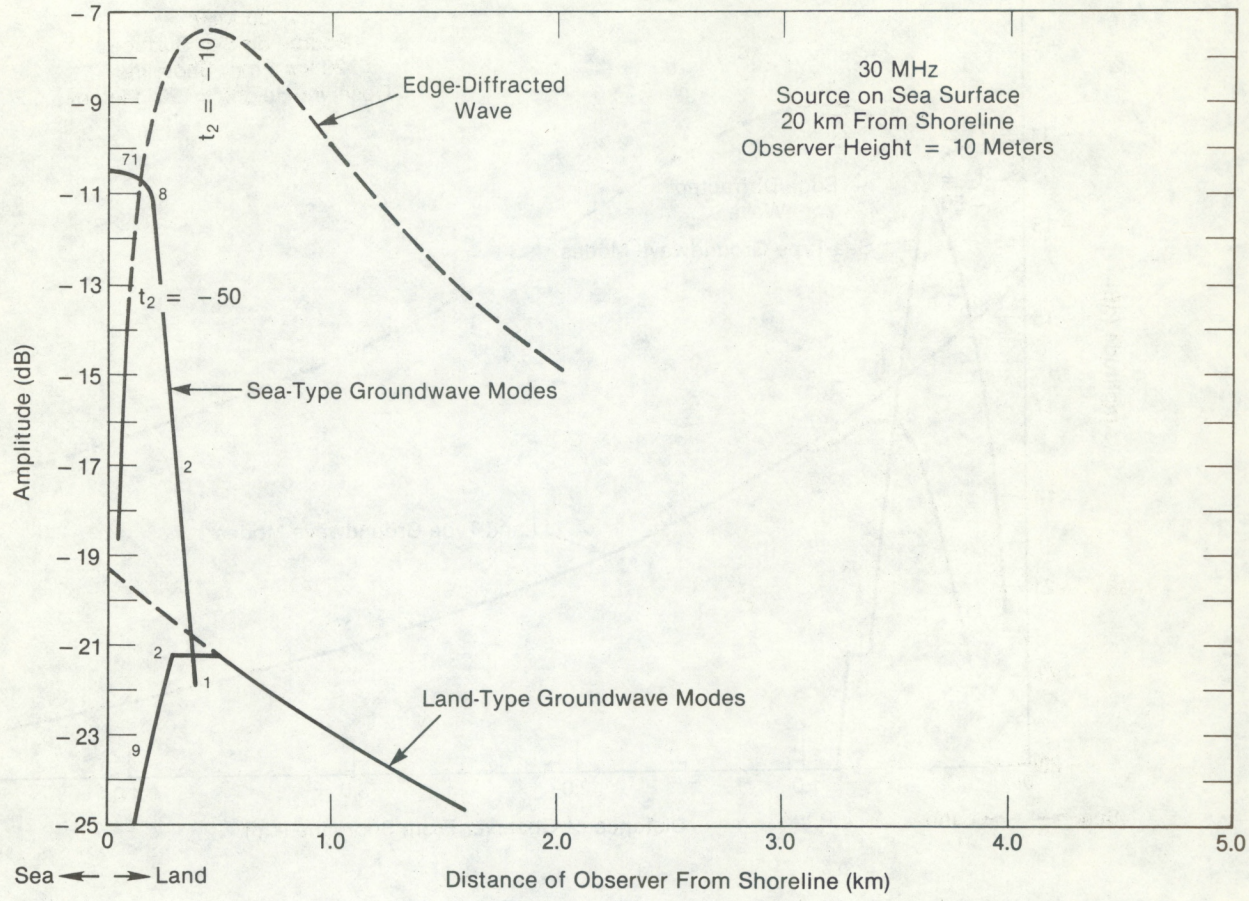

Figure 13. The field near the land-sea interface for an observer 10 m above sea level. The other conditions are the same as in Fig. 12.

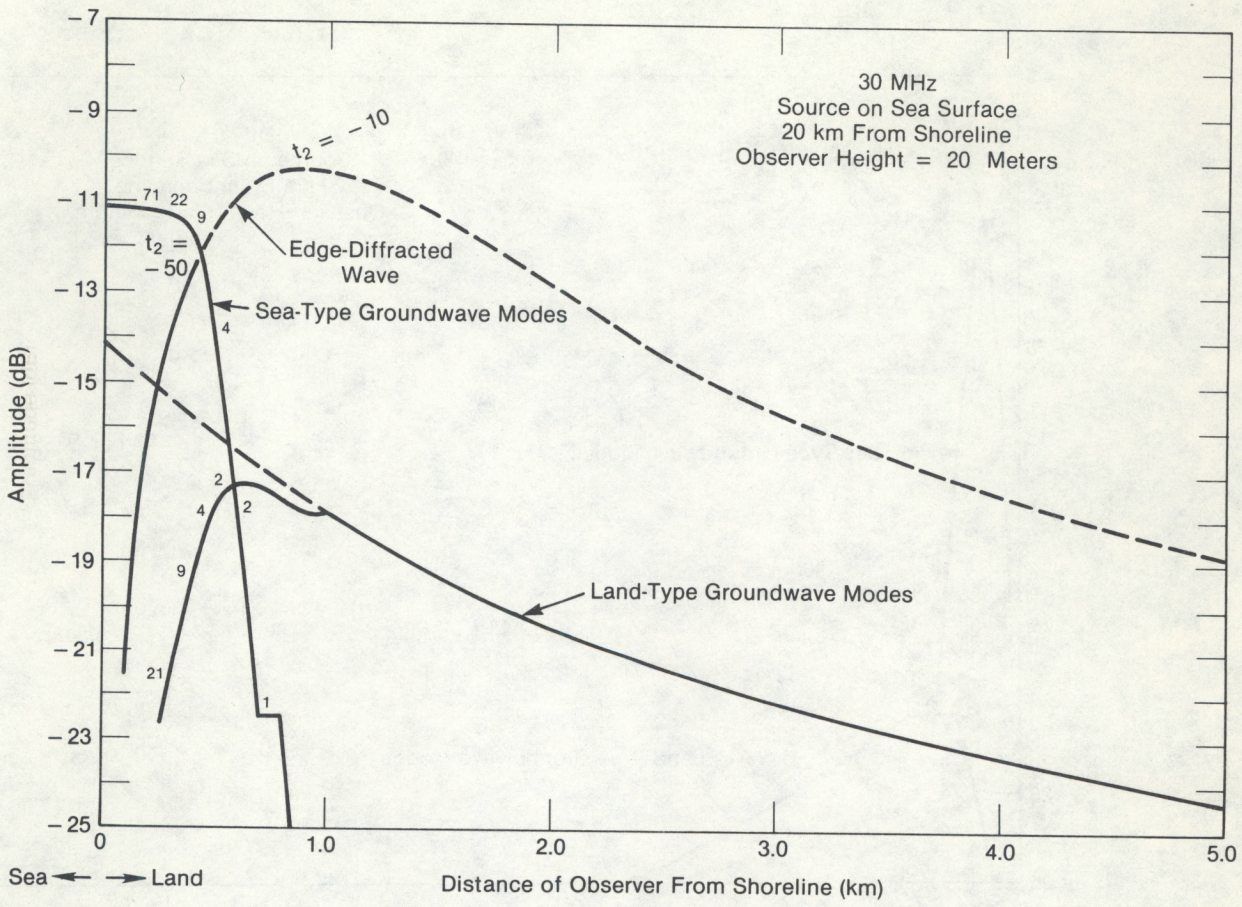

Figure 14. The field near the land-sea interface for an observer 20 m above sea level. The other conditions are the same as in Fig. 12.

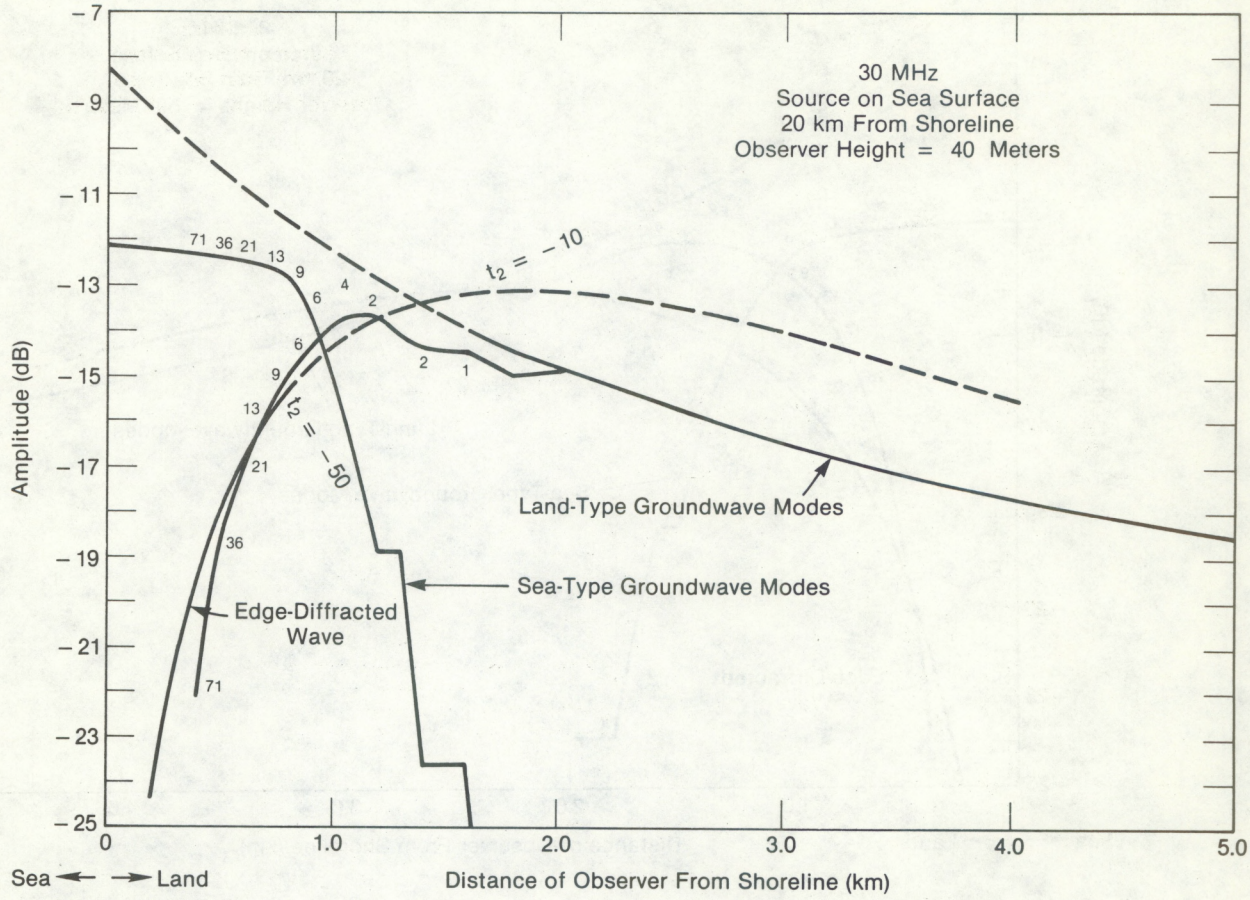

Figure 15. The field near the land-sea interface for an observer 40 m above sea level. The other conditions are the same as in Fig. 12.

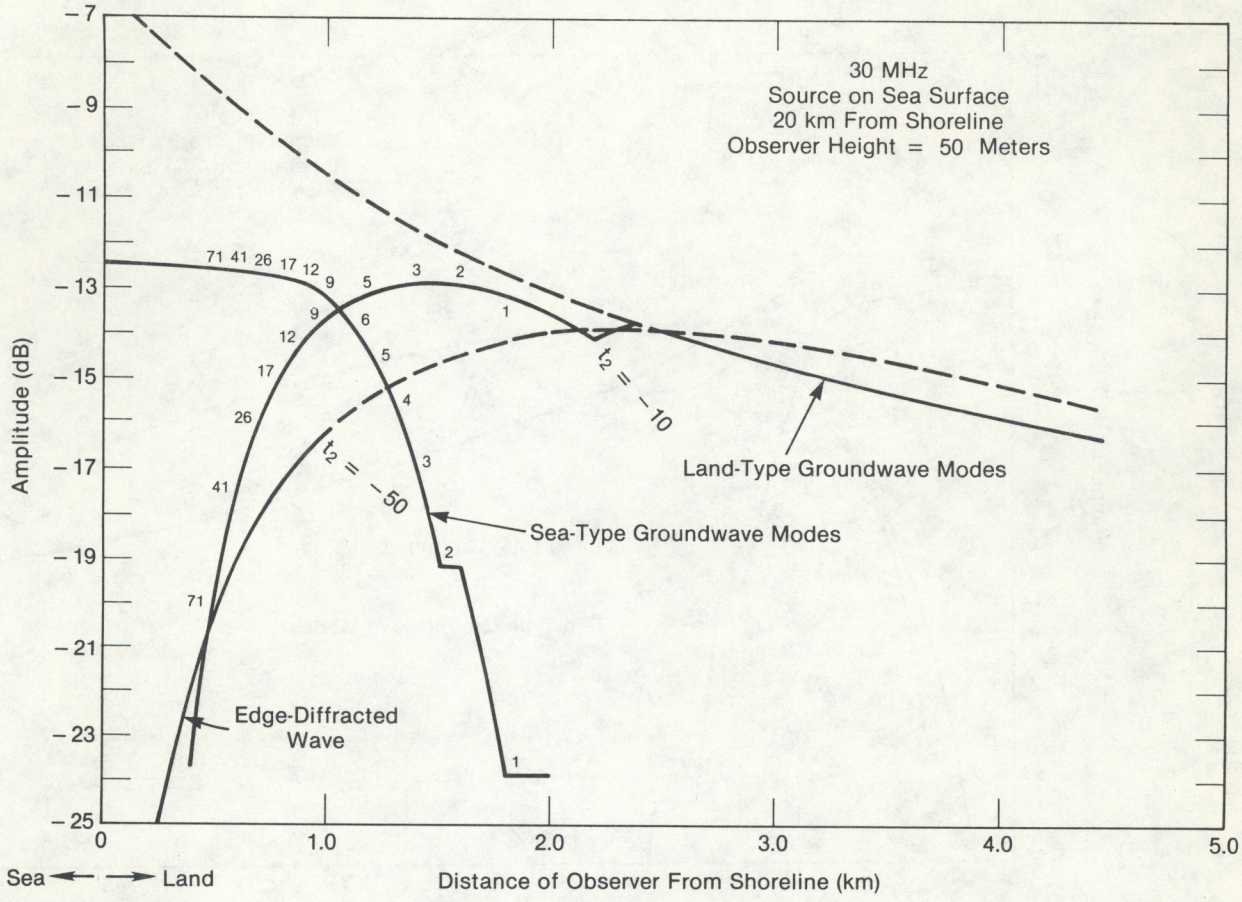

Figure 16. The field near the land-sea interface for an observer 50 m above sea level. The other conditions are the same as in Fig. 12.

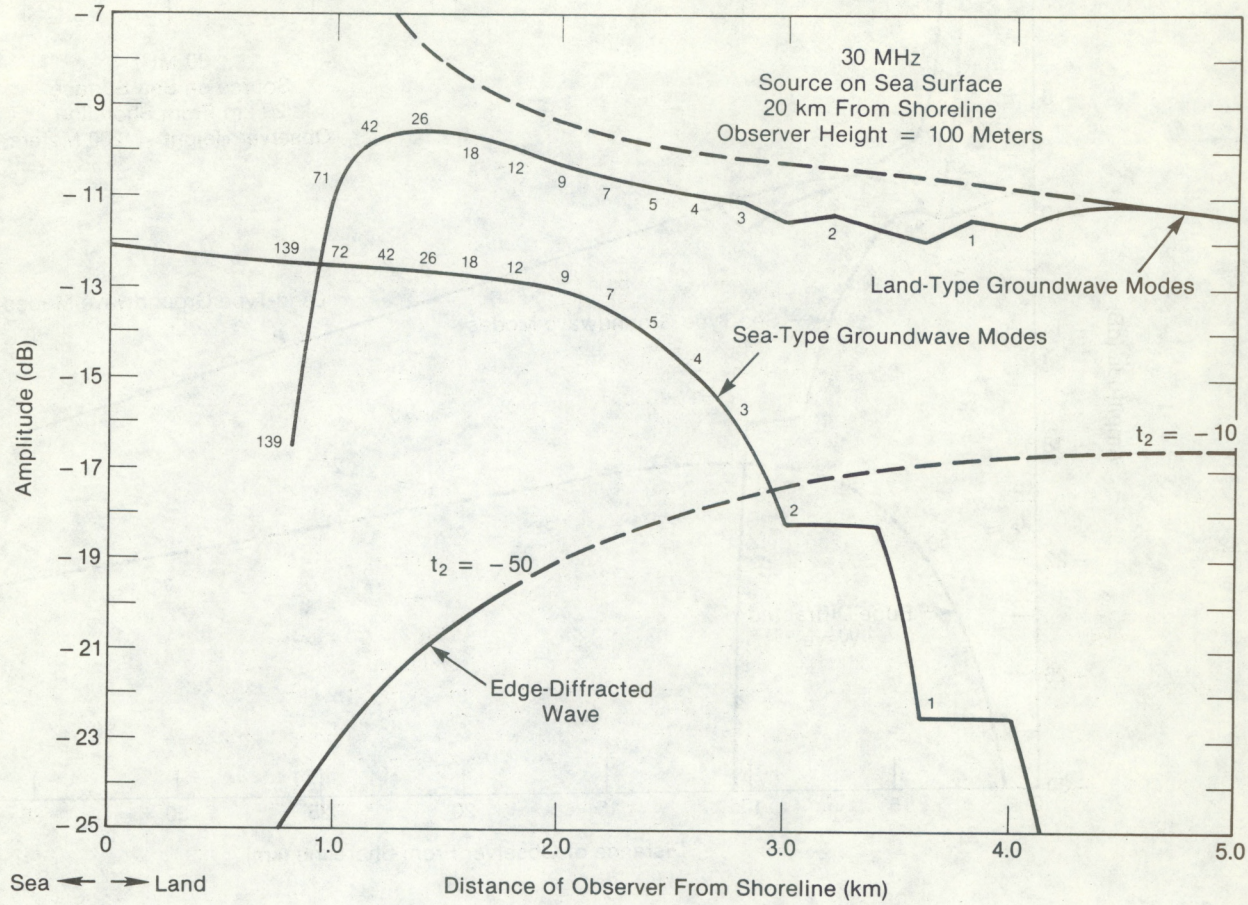

Figure 17. The field near the land-sea interface for an observer 100 m above sea level. The other conditions are the same as in Fig. 12.

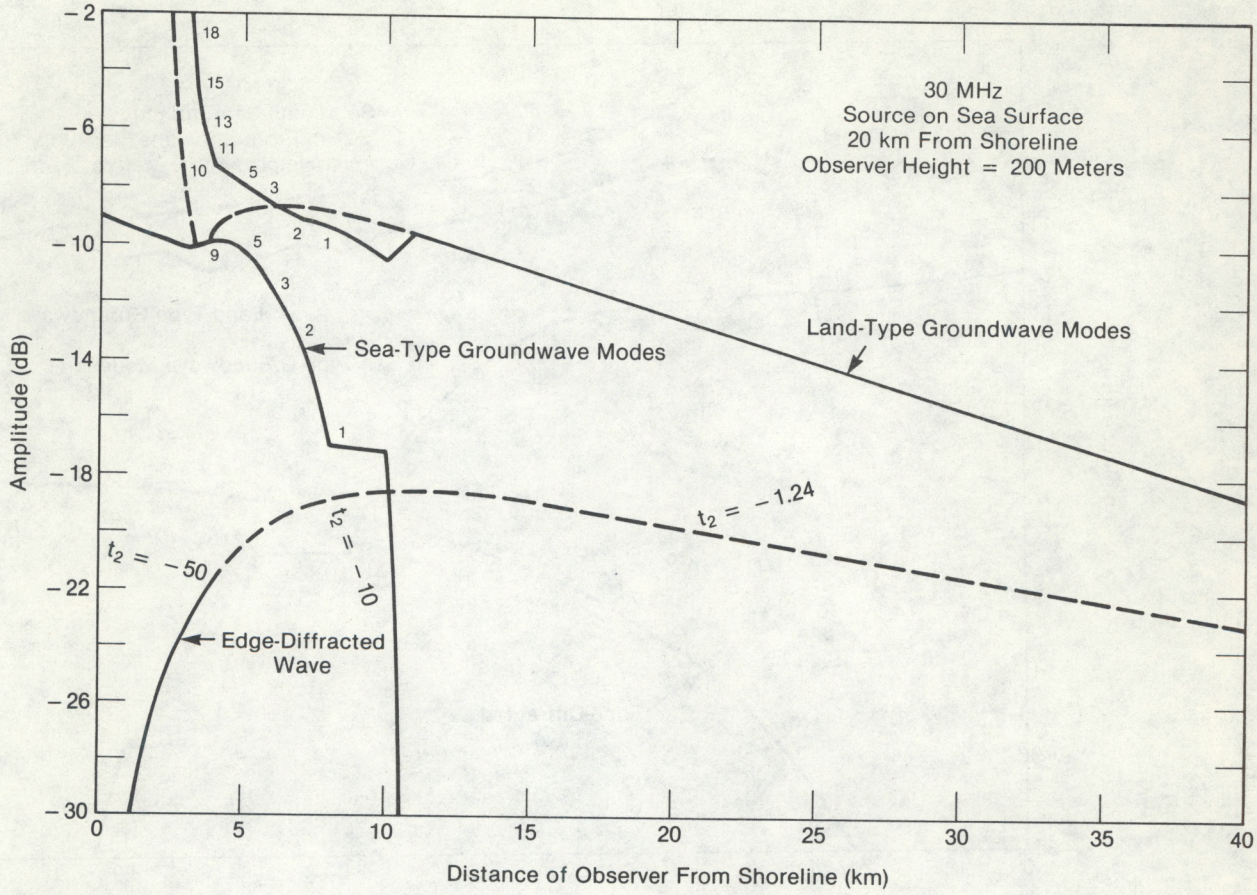

Figure 18. The field near the land-sea interface for an observer 200 m above sea level. The other conditions are the same as in Fig. 12.

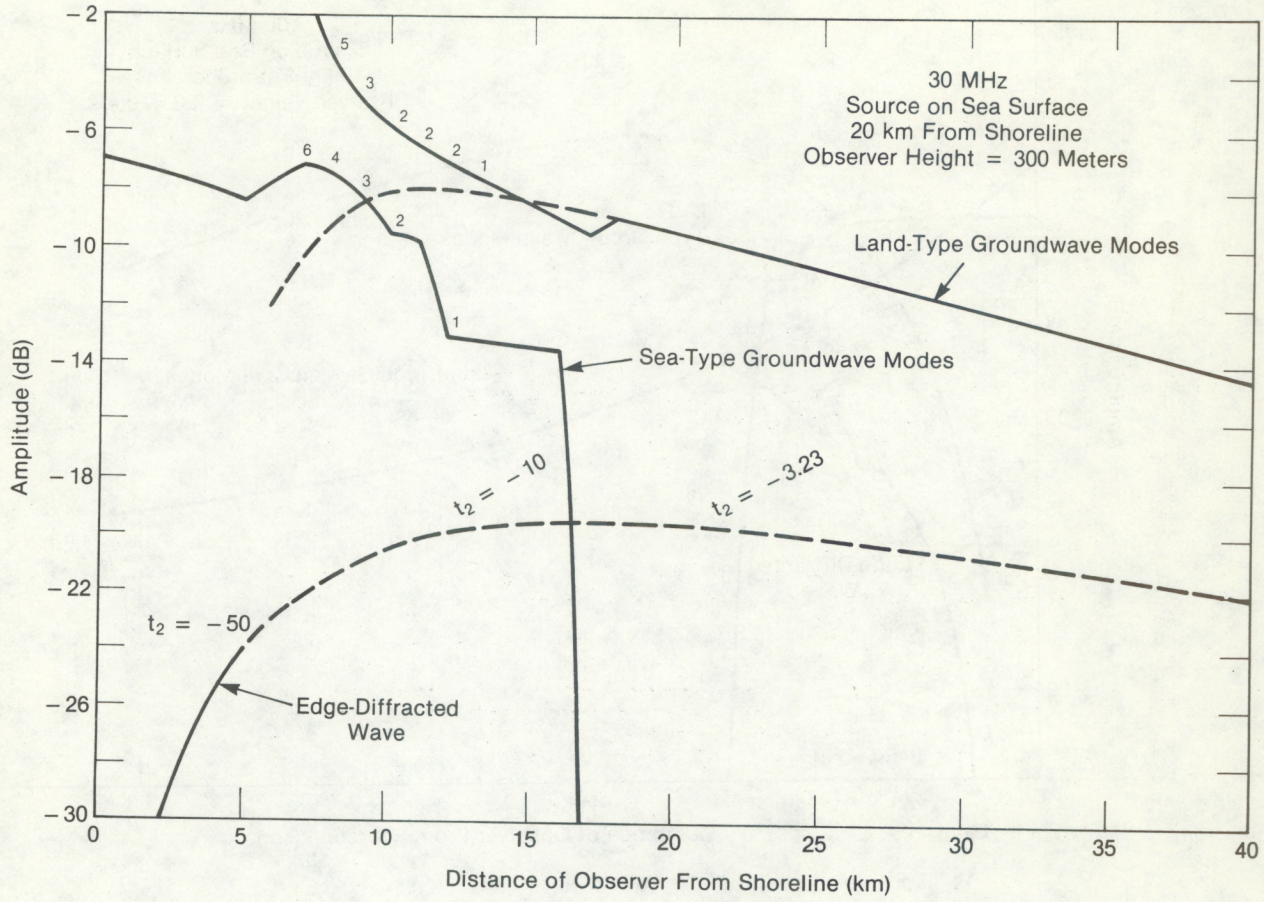

Figure 19. The field near the land-sea interface for an observer 300 m above sea level. The other conditions are the same as in Fig. 12.

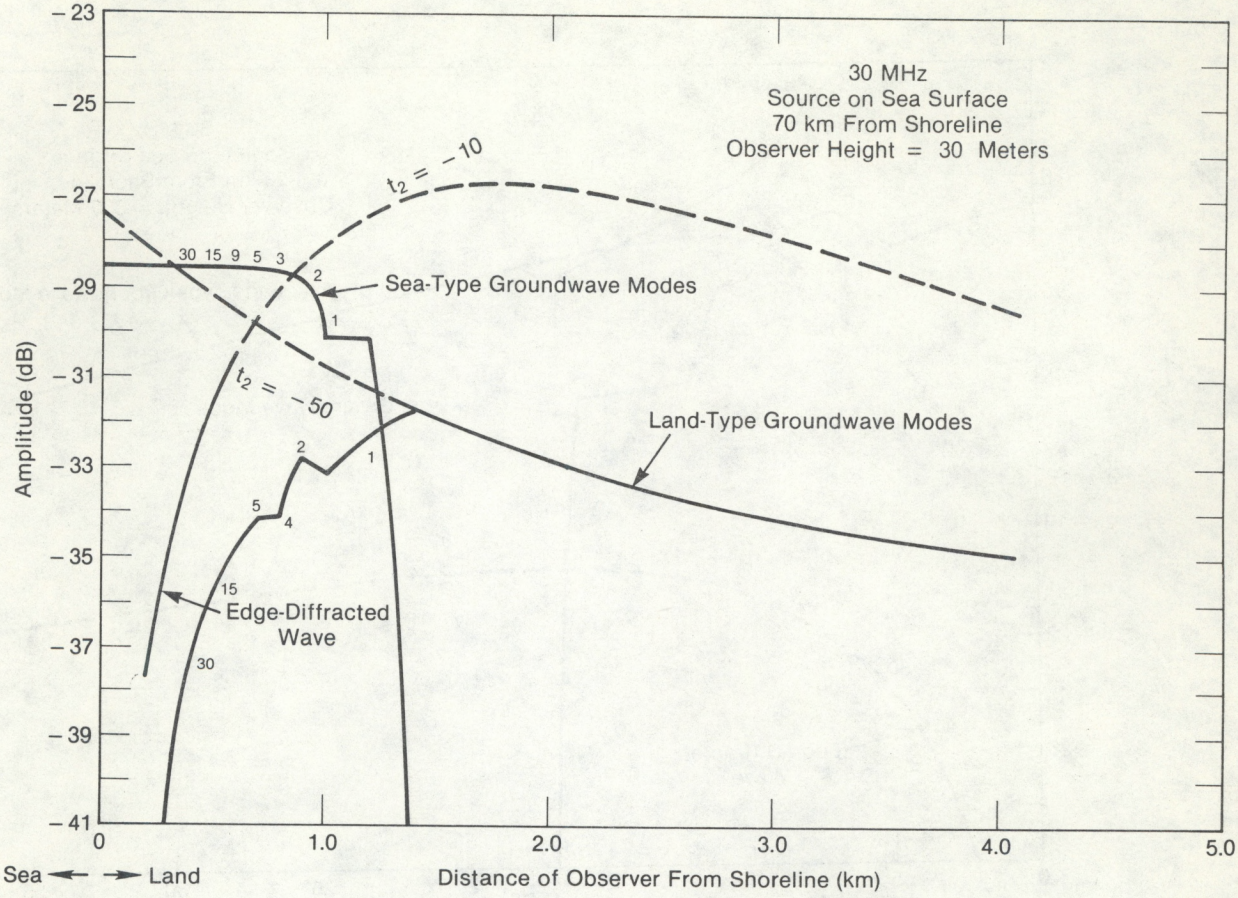

Figure 20. The field near the land-sea interface for an observer 30 m above sea level. The source is a vertical electric dipole on the surface of the sea 70 km from the shoreline. The other conditions are the same as in Fig. 12.

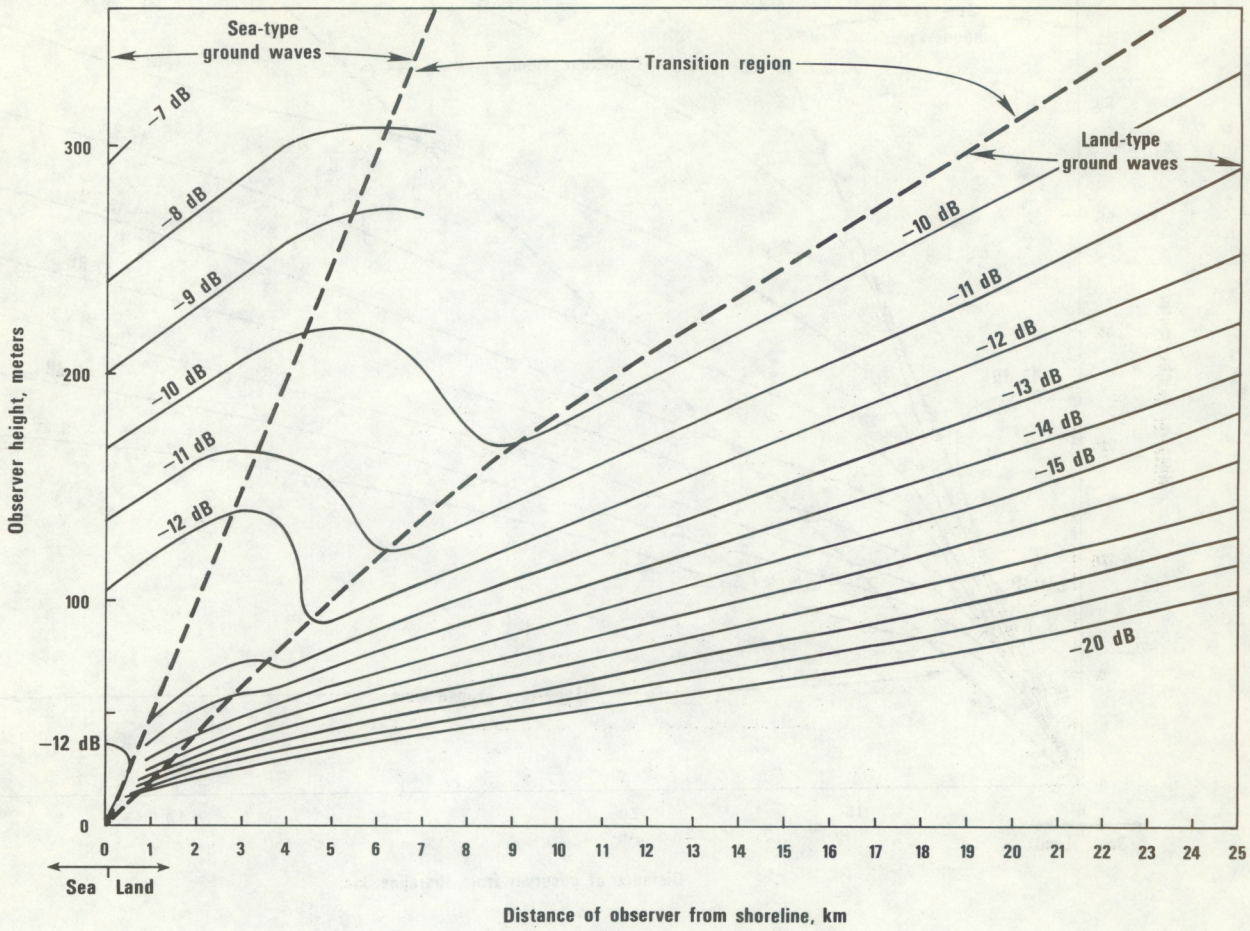

Figure 21. Contours of constant field strength (relative to the free-space field above a flat, perfect conductor) over land near a land-sea interface. The source is a vertical electric dipole on the surface of the sea 20 km from the shoreline. The frequency is 30 MHz. The conditions are the same as those for Figures 12 through 19. The dashed lines separate the three regions: the region where sea-type groundwaves are dominant, the transition region where some modes for both types of groundwaves are in the shadow, and the region where the land-type groundwaves are dominant. The exact shape of the contours in the transition region is uncertain because the exact transition of each groundwave mode across its shadow boundary was not calculated.

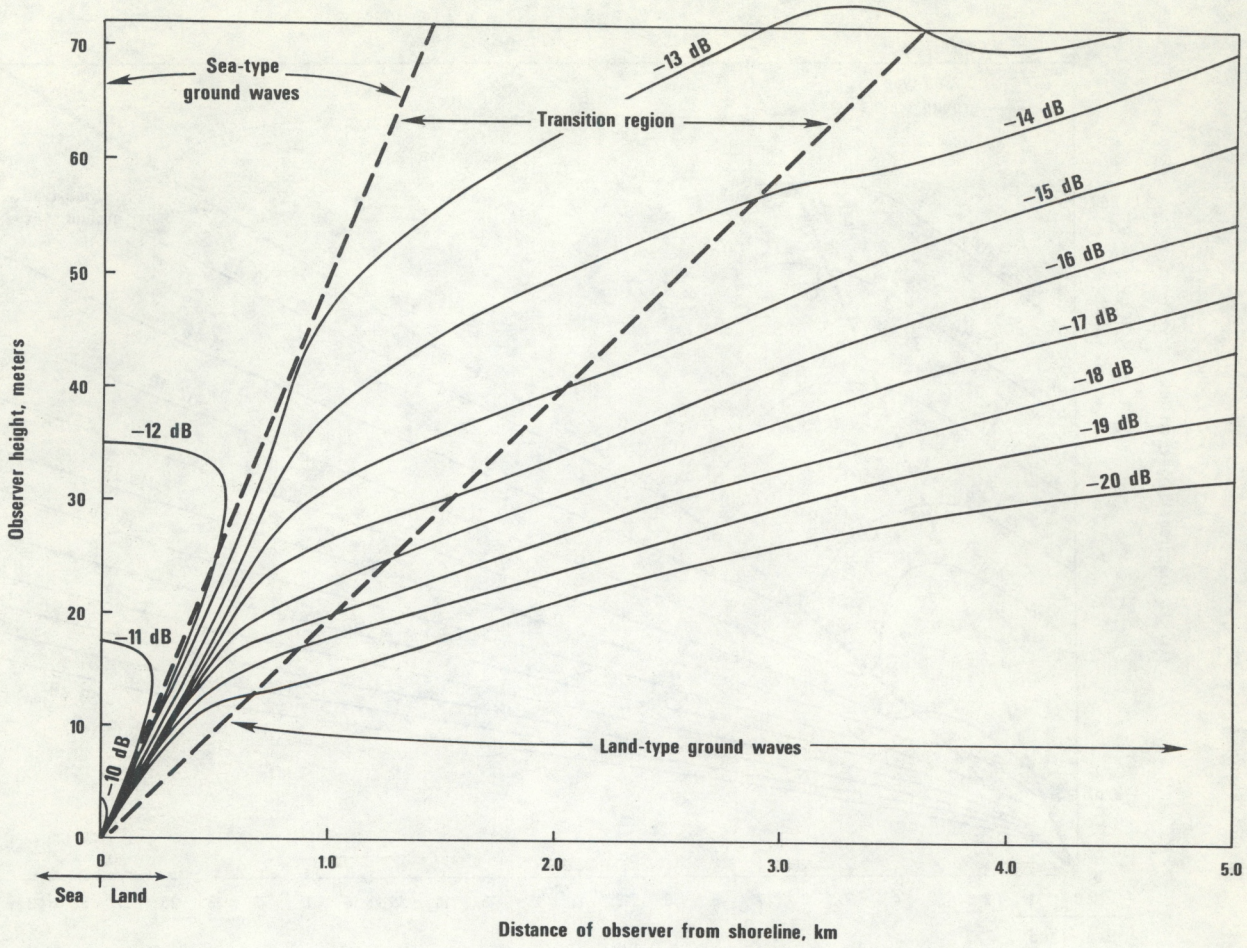

Figure 22. Contours of constant field strength over land near a land-sea interface, as in Fig. 21, but showing more detail near the shoreline.

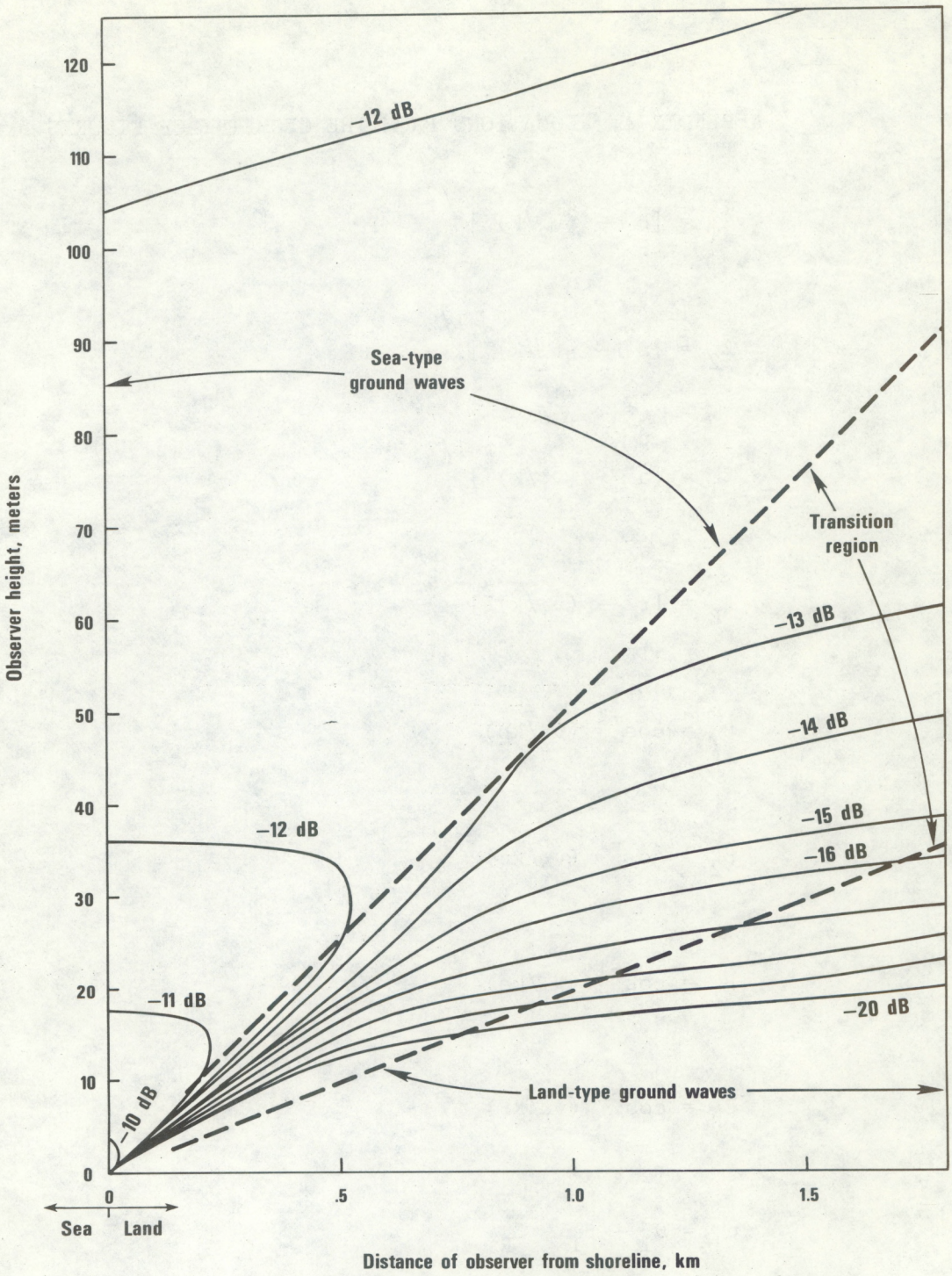

Figure 23. Contours of constant field strength over land near a land-sea interface, as in Fig. 21, but showing more detail near the shoreline.

APPENDIX A. EQUATIONS FROM THE GEOMETRY OF FIGURES 5 AND 7

$$\ell_T = [b^2 - (\nu_2/k)^2]^{1/2} \tag{A.1}$$

$$\ell_2 = [a^2 - (\nu_2/k)^2]^{1/2} \tag{A.2}$$

$$\ell_1 = [a^2 - (\nu_1/k)^2]^{1/2} \tag{A.3}$$

$$\ell_R = [r^2 - (\nu_1/k)^2]^{1/2} \tag{A.4}$$

$$\beta_T = \cos^{-1} (\nu_2/kb) \tag{A.5}$$

$$\beta_2 = \cos^{-1} (\nu_2/ka) \tag{A.6}$$

$$\beta_1 = \cos^{-1} (\nu_1/ka) \tag{A.7}$$

$$\beta_R = \cos^{-1} (\nu_1/kr) \tag{A.8}$$

$$\alpha_1 = \theta_1 - \beta_1 - \beta_R \tag{A.9}$$

$$\alpha_2 = \theta_2 - \beta_T - \beta_2 \tag{A.10}$$

$$\theta = \theta_1 + \theta_2 \tag{A.11}$$

$$\ell = [h^2 + 2\,ar\,\sin^2\theta_1/(1 + \cos\theta_1)]^{1/2} \tag{A.12}$$

$$\phi = \sin^{-1}(a\,\sin\theta_1/\ell) \tag{A.13}$$

$$\beta = \pi/2 - \phi - \theta_1 \tag{A.14}$$

APPENDIX B. EQUATIONS FROM TABLE 1 APPLIED TO FIGURES 5 AND 7

$$\frac{2}{3}(y_b - t_2)^{3/2} = (k^2b^2 - \nu_2^2)^{1/2} - \nu_2 \cos^{-1} \nu_2/kb, \tag{B.1}$$

$$\frac{2}{3}(y - t_1)^{3/2} = (k^2r^2 - \nu_1^2)^{1/2} - \nu_1 \cos^{-1} \nu_1/kr, \tag{B.2}$$

$$\nu_2 = ka + \left(\frac{ka}{2}\right)^{1/3} t_2, \tag{B.3}$$

$$\nu_1 = ka + \left(\frac{ka}{2}\right)^{1/3} t_1, \tag{B.4}$$

$$q_2 = -i\left(\frac{ka}{2}\right)^{1/3} z_2/\eta_o = -i\left(\frac{ka}{2}\right)^{1/3} \Delta_2, \tag{B.5}$$

$$q_1 = -i\left(\frac{ka}{2}\right)^{1/3} z_1/\eta_o = -i\left(\frac{ka}{2}\right)^{1/3} \Delta_1, \tag{B.6}$$

z_2 and z_1 are the surface impedances of the sea and land, η_o is the impedance of free space, and t_2 and t_1 are determined by

$$w_1'(t_2) = q_2 w_1(t_2) \tag{B.7}$$

and

$$w_1'(t_1) = q_1 w_1(t_1) \tag{B.8}$$

APPENDIX C. DEFINITIONS

$$x_2 \equiv (ka/2)^{1/3}\theta_2 \tag{C.1}$$

$$x_1 \equiv (ka/2)^{1/3}\theta_1 \tag{C.2}$$

$$x \equiv (ka/2)^{1/3}\theta = x_1 + x_2 \tag{C.3}$$